Fluorescence Correlation Spectroscopy Studies of Polymer Systems

Dominik Wöll

Contents

D. Wöll (✉)
Institute for Physical Chemistry, RWTH Aachen University, Landoltweg 2, 52074 Aachen, Germany
e-mail: woell@pc.rwth-aachen.de

Abstract This chapter discusses the potential of fluorescence correlation spectroscopy (FCS) to study polymer systems. It introduces the technique and its variations, describes analysis methods, points out advantages and limitations, and summarizes FCS studies of molecular and macromolecular probes in polymer solutions, polymer gels, polymer nanoparticles, and polymeric micellar systems. In addition, a comparison with other experimental methods is presented and the potential of a combination with simulations discussed.

Keywords Fluorescence correlation spectroscopy • Fluorescence microscopy • Fluorescent probes • Polymer solutions • Polymer gels • Polymer nanoparticles • Polymeric micellar systems • Translational diffusion

1 Introduction

Fluorescence correlation spectroscopy (FCS) is a powerful method to measure the timescales of dynamics within different environments and allows for a determination of some photophysical properties of the fluorescent probes. Even though most studies have so far addressed biological questions, FCS could also give valuable insights into polymer systems [1]. Its particular advantages are that it allows for measurements with only minor sample amounts. Since the labeling concentrations are very low, a significant disturbance of the systems can be excluded. Thus, structures and their dynamics can be resolved in situ with a good spatial resolution at the diffraction limit of optical light, i.e., on a sub-μm length scale. The elucidation of diffusional processes on this scale is essential for a deeper understanding of the relationship between polymer structure and dynamics and its manifestation on the macroscopic properties of the polymer. The complexity of this relationship challenges all experimental and theoretical methods, and only combining their strengths will allow us to gain a consistent picture of polymers from the nanoscopic to the microscopic scale. Unraveling these secrets is still amongst the very dreams of polymer scientists and probably can foster the development of novel sophisticated functional materials with tunable properties.

This book chapter is intended to review the current state of the art of FCS and to emphasis the advantages, but also the limits of this technique for the measurement in polymer systems. It will discuss analysis methods for FCS data and point out the potential of FCS for future studies on polymers and their applications.

2 FCS Measurements and Analysis

2.1 FCS Setup

Already in 1972, Magde, Webb, and Elson published the first paper on fluorescence correlation spectroscopy yielding chemical rate constants and diffusion coefficients [2], followed by a series of further reports on these novel techniques [3–5]. However, several further developments were necessary for FCS to reach its current power which has been reviewed several times as for example in [6–10]. One key step in the evolution of FCS was its combination with confocal microscopy to enhance spatial resolution basically down to the diffraction limit of the fluorescence light and the concomitant increase in sensitivity [11]. Further important technical improvements concern the quality of optical components and the sensitivity and time resolution of detectors. Additionally, better labels and labeling strategies have become available, a point which should not be underestimated.

In a typical FCS experiment, as shown in Fig. 1, a collimated laser beam is focused by an objective lens into a diffraction-limited confocal volume within the sample placed on a glass cover slide. Part of the light emitted from this confocal volume is collected by the same objective and separated from excitation light using a dichroic mirror and an emission filter. The emission light is focused onto a pinhole blocking most of the light not originating from the confocal volume, thereby, as shown in Fig. 2, improving mainly the axial z-resolution. However, to a minor extent, also the lateral x- and y-resolution are improved. This way, the overall size of the confocal volume typically can be reduced to ca. 0.1 femtoliter. The photons passing through the pinhole are detected with a photo detector, typically an avalanche photo diode (APD). Such APDs possess good quantum efficiencies and, with appropriate electronics, allow for the determination of the arrival times of single photons with an accuracy in the picosecond range.

2.2 Autocorrelation Analysis

The number of detected photons within a certain time interval is typically binned and determines the measured fluorescence intensity. This intensity fluctuates on different timescales caused by different diffusional, photochemical, or photophysical processes. The timescales of these processes can be most straight-forward analyzed using the autocorrelation function

$$G(\tau) = \frac{\langle \delta I(t) \cdot \delta I(t+\tau) \rangle}{\langle I(t) \rangle^2} = \frac{\langle I(t) \cdot I(t+\tau) \rangle}{\langle I(t) \rangle^2} - 1 \qquad (1)$$

of the fluorescence intensity $I(t)$ or its deviations $\delta I(t) = I(t) - \langle I(t) \rangle$ from the mean intensity. This function describes the (average) correlation between the
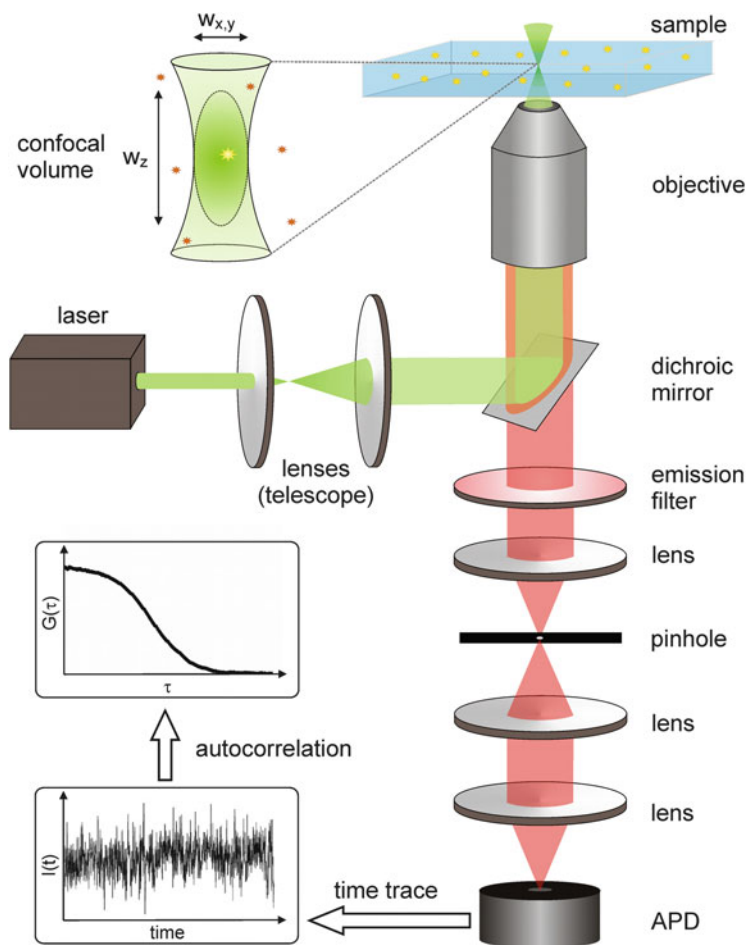
Fig. 1 Typical FCS setup (figure reproduced and adapted from Wöll [1] with permission of The Royal Society of Chemistry)

intensity at a time t with the intensity at a time shifted by the time interval τ. It can be interpreted as the conditional probability density of detecting photons, provided one photon is detected at zero time. The autocorrelation function contains information about the timescale of all processes that cause fluctuations in the fluorescence intensity.

Translational diffusion can be typically observed on timescales longer than 0.1 millisecond. In the µs range, the autocorrelation function often drops due to triplet blinking [12]. After excitation, the fluorophore undergoes intersystem crossing from a singlet (typically S_1) to a triplet state (typically T_1) and remains dark during the lifetime of this triplet state before it relaxes back to the singlet system, where it can fluoresce again by cycling between the S_0 and the S_1 states.
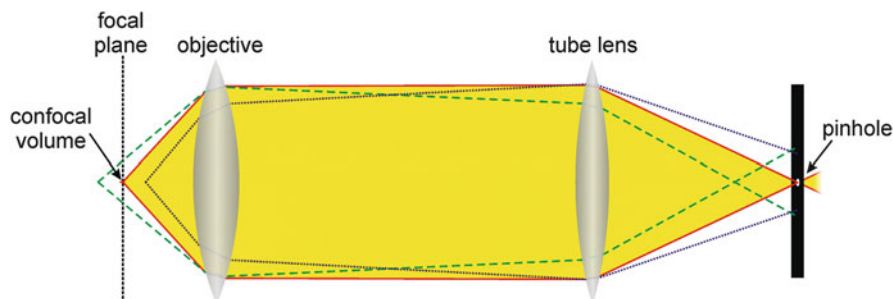
Fig. 2 Effect of the pinhole on the axial resolution of a confocal microscope. Only light originating from the confocal volume (*red solid line*, *yellow area*) can pass the pinhole without loss. Light from planes further away from the objective (*green dotted line*) focuses already in front of the pinhole (*green dotted line* and *blue dotted line*) and, thus, is mainly blocked, whereas light from planes closer to the objective is not yet focused at the plane of the pinhole and, therefore, most of this light also cannot pass (figure reproduced from Wöll [1] with permission of The Royal Society of Chemistry)

Photoisomerizations between two states with different fluorescence intensities can also be observed in the μs range [13]. The fast photophysics within different singlet states, i.e., the excitation from the singlet ground state and the emission of a fluorescence photon from an excited singlet state, are determined by the absorption cross section, the light intensity, and the fluorescence lifetime. This causes an intensity increase within nanoseconds which is called antibunching [14]. For concentrations with statistically less than one fluorescence molecule in the confocal volume, it is impossible to observe two fluorescence photons instantaneously because after one photon has been emitted, the fluorophore is in the electronic ground state. It requires time to be excited again and to emit a second photon. Thus, the autocorrelation functions approach a value of zero for very short (sub-ns) time intervals. Finally, rotational motion of single molecules with a well-defined transition dipole moment also causes intensity fluctuations. They can span a rather large timescale between sub-nanoseconds and milliseconds depending on the viscosity of the medium and even stronger on the probe size, since, according to the Stokes–Einstein–Debye equation, the rotational diffusion coefficient of a probe is indirectly proportional to the third power of its radius. However, care has to be taken when the fluorophore is part of a larger probe molecule and can reorient independently within this molecule. In this case, the fluorophore does not reflect the rotational motion of the probe but a complex combination of probe rotation and its own reorientation within the probe molecule.

The autocorrelation curve can then be fitted to autocorrelation functions calculated using reasonable models for the respective processes which are in detail explained in Chapter 5 of the "Handbook of Fluorescence Spectroscopy and Imaging" [15]. Here, we rather concentrate on providing the formulas typically used for fitting.

2.3 Analysis of Translational Diffusion

Translational diffusion can be described by a model with a 3D Gaussian intensity profile of the confocal volume which possesses the same width w_{xy} in the lateral x- and y-direction but a different width w_z in the axial z-direction. This can be related to the autocorrelation [see Eq. (1)] using the following equation:

$$G_{tr}(\tau) = \frac{1}{N}\left(1 + \frac{\tau}{\tau_D}\right)^{-1}\left(1 + \left(\frac{w_{xy}}{w_z}\right)^2\frac{\tau}{\tau_D}\right)^{-\frac{1}{2}} \tag{2}$$

wherein N is the average number of fluorescent probes in the confocal volume and τ_D is the diffusional correlation time. The square root term corrects for the difference of the axial and lateral size of the elliptical confocal volume. Typical values are ca. 300 nm for w_{xy} and ca. 1.5 µm for w_z.

The highest sensitivity for the determination of τ_D is realized when the confocal volume contains in average approximately one independently diffusing probe, which is the case for sub-nanomolar concentrations. If the probe concentration is too low, the events of a probe diffusing through the confocal volume become rather seldom and (random) background noise will dominate the signal resulting in no correlation to be detectable. For much higher concentrations, the relative intensity of the fluctuations of the fluorescence signal becomes less, and thus the sensitivity of FCS decreases. However, it has been recently shown that with a high count rate detector system and applying laser fluctuation corrections, FCS diffusion measurements were possible even with fluorescent probe concentrations in the µM range [16].

The correlation time τ_D depends on the exact dimensions of the confocal volume and is therefore not a quantity to compare translational motion in different systems with each other. Therefore, in most cases, the diffusion coefficient D is calculated using Einstein's mean square displacement

$$\tau_D = \frac{4D}{w_{xy}^2} \tag{3}$$

which results in

$$G_{tr}(\tau) = \frac{1}{N}\left(1 + \frac{4D\tau}{w_{xy}^2}\right)^{-1}\left(1 + \frac{4D\tau}{w_z^2}\right)^{-\frac{1}{2}} \tag{4}$$

The dimensions w_{xy}^2 and w_z^2 have to be determined by a reference measurement. For aqueous systems, a common and reliable reference is rhodamine 6G (Rh6G) in water with a diffusion coefficient of 4.14×10^{-10} m^2 s^{-1} [17]. The ratio w_z^2/w_{xy}^2 is typically in the range between 5 and 8. The diffusion coefficient D can be used to

determine the hydrodynamic radii of diffusing molecules, nanoparticles, or aggregates using the Stokes–Einstein equation

$$r_{h} = \frac{k_{B}T}{6\pi\eta D} \tag{5}$$

with the Boltzmann constant k_{B}, the sample temperature T, and the viscosity η.

It should however be kept in mind that Eqs. (2) and (4) only describe translational diffusion, if the shape of the focal spot convoluted with the detection efficiency profile is Gaussian, and if the emitters are point like. Micelles or other aggregates with multiple labels distributed over the whole nanoparticle require an analysis using the form factor of the distribution of labels on the particle [18]. Furthermore, in order to obtain reliable diffusion coefficients for complex systems, it has been reported that the minimum lag time, the maximum lag time, and the averaging time are critical parameters which have to be chosen appropriately [19].

If several independent diffusants with different diffusion coefficients are present in the sample, the autocorrelation function can be approximated by the summation of the terms of Eq. (4):

$$G_{tr}(\tau) = \frac{1}{N}\sum_{i=1}^{n} f_i \cdot Q_i^2 \cdot \left(1 + \frac{4D_i\tau}{w_{xy}^2}\right)^{-1} \left(1 + \frac{4D_i\tau}{w_z^2}\right)^{-\frac{1}{2}} \tag{6}$$

where D_i are the individual diffusion coefficients of the species i with a number fraction of f_i and a fluorescence quantum yield of Q_i. If the individual diffusion coefficients differ by more than an order of magnitude, they can be unambiguously identified as distinct shoulders in $G(\tau)$. A smaller difference makes it difficult to distinguish individual contributions. In principle, if it spans several orders of magnitude, the distribution of D_i's can be yielded using a maximum entropy method [20] or a multicomponent analysis using the CONTIN algorithm [21]. Yet, the statistical quality of the measured $G(\tau)$ is the limiting factor of such types of analysis.

2.4 Analysis of Anomalous Diffusion

Another challenge is the analysis of anomalous diffusion from FCS measurements. Deviations from normal diffusion can be caused by internal chain motions [22–24] of (bio-)polymers, by molecular crowding [24–30], or by the restriction of diffusion to a certain "corral" region [31]. Different approaches have been suggested to deal with anomalous diffusion. One of the possibilities to describe anomalous diffusion uses a power law scaling of time τ^{α} [23, 26, 29, 30, 32, 33]. The scaling parameter α can depend on the timescale investigated and thus allows for a distinction between

translational and chain diffusion [22]. The ensemble average mean square displacement (MSD) $\langle \Delta r^2(\tau) \rangle$ with time τ can thus be expressed as follows:

$$\langle \Delta r^2(\tau) \rangle = 6D\tau^\alpha \tag{7}$$

If the probability distribution of displacements is Gaussian, the exponent α can be obtained by a combination of Eqs. (7) and (4) yielding [34]

$$G_{\mathrm{tr}}(\tau) = \frac{1}{N} \left(1 + \frac{2\langle \Delta r^2(\tau) \rangle}{3w_{xy}^2} \right)^{-1} \left(1 + \frac{2\langle \Delta r^2(\tau) \rangle}{3w_z^2} \right)^{-\frac{1}{2}} \tag{8}$$

Using this approach, the internal dynamics of long DNA molecules was studied and discussed in the framework of theories for polymer dynamics [35–37]. Different scaling regimes with exponents α of 2/3 and 1 were found for the internal dynamics at intermediate timescales and the crossover to the diffusion of the whole chain at long timescales, respectively. It has however been carefully checked whether the assumptions for using Eq. (8) are justified by the underlying microscopic model of diffusion. Without the verification by such a specific microscopic model, false conclusions might be drawn about subdiffusive behavior [38]. In general, single particle or single molecule tracking are more suitable to distinguish between different types of diffusion [39]. For a non-Gaussian distribution of displacements, Höfling et al. [40] derived a relation between the particle trajectory and autocorrelation function $G(t)$. This, however, requires information about entire trajectories and the averaged information from FCS experiments is not sufficient for its application.

Apart from the abovementioned analytical tools, a technical approach to detect anomalous diffusion has been reported. Sample-volume-controlled-(SVC-) FCS can directly detect anomalous diffusion by changing the diameter of the collimated excitation laser beam [41, 42]. One of the challenges of this approach is however the control over the optical parameters such as distortions of the confocal volume [43].

At constant focus size, it was shown that FCS cannot distinguish between diffusion constrained by elastic force, walking confined diffusion, and hop diffusion averaged over many measurements [44]. The simulations indicate that the mean square displacements of all these types of restricted diffusion can reliably be interpreted using one archetypal model presented by the following equation:

$$\langle \Delta r^2(\tau) \rangle = 6D_{\mathrm{L}}\tau + \frac{6}{5}a^2 \left(1 - \exp\frac{-\gamma(5D_{\mathrm{S}}\tau)}{a^2} \right) \tag{9}$$

wherein D_{L} and D_{S} present the (macroscopic) diffusion coefficient measured for long time intervals and the (microscopic) diffusion coefficient measured for short time intervals, respectively. Equation (9) is only valid if the D_{L} and D_{S} are sufficiently well separated. Furthermore, a is an effective confinement radius and γ an exponential decay constant which depends on the model used ($\gamma = 1$ for diffusion constrained by elastic force, $\gamma \approx 0.866$ for walking confined diffusion, and $\gamma \approx 0.822$ for hop diffusion).

It should be emphasized at this point that FCS correlation curves can be often fitted equally well by an anomalous diffusion model and using two diffusion time constants. However, it has to be carefully analyzed which of the two models is more appropriate. Combining FCS results with simulations [45], Vagias et al. [46] for example showed that for the case of attractive tracer–polymer interactions, only a two-component diffusion process is a physically meaningful model.

2.5 Full Correlation FCS to Detect Triplet Kinetics, Rotational Diffusion, and Fluorescence Antibunching

In addition to translational diffusion, FCS is in principle also capable of determining the timescale of any process which causes fluctuations of the fluorescence signal. These processes are in particular triplet kinetics, isomerization, rotational diffusion, and fluorescence antibunching. Their timescales are typically shorter than the one of translational diffusion. One technical problem for measuring correlations on such short timescales is that measurements with one APD possess a dead time in the μs range, i.e., the detector is "blind" for this time interval after the detection of one photon. Therefore, any information about correlation of photons on a shorter timescale is lost. Additionally, depending on the detectors used, afterpulsing might cause artifacts. In order to obtain correlation values at shorter timescales, a Hanbury Brown and Twiss setup [47] can be used which splits the emission light and detects the photons on two independent detectors [48, 49]. Cross-correlation of the photon arrival times on the two detectors enables full correlation fluorescence correlation spectroscopy (fcFCS) measurements from the time range of picoseconds to the several minutes which can result in cross-correlation curves as presented in Fig. 3.

Fig. 3 Example of a full correlation FCS curve. The following parameters [see Eq. (10)] were used to simulate antibunching (*blue*), and correlation drops due to rotational diffusion (*cyan*), triplet blinking (*green*), and translational motion (*red*): $\tau_{AB} = 10^{-9}$ s; $\tau_R = 10^{-8}$ s; $R = 1$; $\tau_T = 10^{-5}$ s; $f_T = 0.2$; $\tau_D = 10^{-2}$ s; $\omega = 7$; $N = 1$
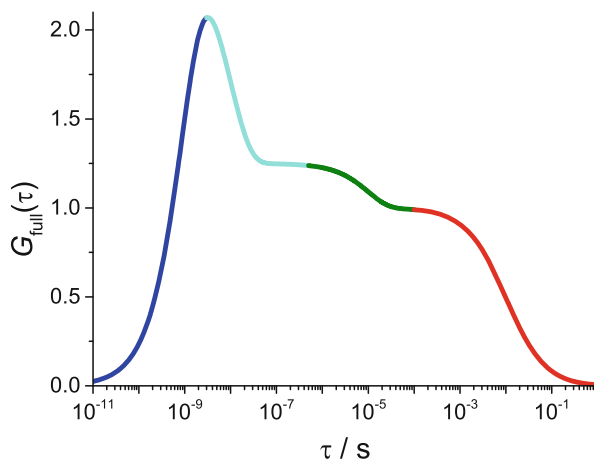
It was shown that for processes well separated in time, the correlation function can be simplified by factorization [50]. Therefore, the curve in Fig. 3 was constructed using the following combined equation with terms for translational diffusion, triplet blinking, rotational diffusion, and antibunching (each process in the corresponding line):

$$
\begin{aligned}
G_{\text{full}}(\tau) = \frac{1}{N}\left(1 + \frac{\tau}{\tau_{\text{D}}}\right)^{-1}\left(1 + \frac{\tau}{\omega^2 \tau_{\text{D}}}\right)^{-\frac{1}{2}} \\
\cdot \left(1 + \frac{f_{\text{T}}}{1 - f_{\text{T}}} \cdot \exp\left(-\frac{\tau}{\tau_{\text{T}}}\right)\right) \\
\cdot \left(1 + R \cdot \exp\left(-\frac{\tau}{\tau_{\text{R}}}\right)\right) \\
\cdot \left(1 - \exp\left(-\frac{\tau}{\tau_{\text{AB}}}\right)\right)
\end{aligned}
\tag{10}
$$

wherein N is the average number of independent emitters in the confocal volume, τ_{D} the translational diffusion time, ω a geometric factor (the ratio between axial and lateral diameter of the ellipsoid confocal volume), f_{T} the triplet fraction, τ_{T} the triplet lifetime, τ_{R} the rotational diffusion time, R the rotational amplitude, and τ_{AB} the antibunching time.

In the following we want to comment on the contribution of rotational diffusion. The theory to analyze rotational diffusion from FCS measurements was developed by Ehrenberg and Rigler [51] and Aragon and Pecora [52, 53]. Strictly spoken, the third term of Eq. (10) is only valid for the rotation of a spherical rotor with parallel transition dipole moments for absorption and emission and also with the same hydrodynamic properties in the ground and in the excited state. Furthermore, only the term with quantum number $l = 2$ of the angular momentum operator $\mathbf{L}^2$ has been considered [52, 54]. The sensitivity to measure rotational diffusion coefficients depends also on the polarization settings of the FCS setup, as nicely documented by Enderlein and coworkers [55, 56].

3 Technical Variations of FCS

As in most other experimental techniques, there is also a constant development and improvement involved in FCS which broadens its range, applicability, and accuracy. These developments resulted in advances such as dual-focus FCS, total internal reflection FCS, and STED-FCS which will be discussed in this section. Apart from this progress, a multitude of other variations have been reported which cannot be covered within this book chapter. These include FCS with two-photon excitation [57–61], spatial fluorescence cross-correlation spectroscopy (FCCS) which can be used to investigate microflows [62], dual-color FCCS to correlate

the fluctuations from two spectrally distinct fluorophores in order to analyze kinetics or association [63], pulsed interleaved excitation (PIE) FCS [56, 64], fluorescence triple correlation spectroscopy (F3CS) [65], and filtered FCS [66].

One of the main tasks in FCS is to obtain the maximum amount of (useful) information from the fluorescence light with reasonable effort and costs. Therefore, as many photons as possible should be detected including their parameters such as polarization, color, detection time, etc. [67]. Improvements have, however, not only been restricted to an improved detection of photons and their parameters, but also implemented new excitation and detection geometries.

3.1 Dual-Focus FCS

Enderlein and coworkers introduced dual-focus FCS (2fFCS) [68] in which two laser foci are alternately excited and detected. The distance between both laser foci serves as an internal distance reference, i.e., an intrinsic ruler. This avoids reference measurements which are otherwise necessary to relate diffusion time and diffusion coefficient. The accuracy of the obtained diffusion coefficients is sufficiently high to allow for sensitive measurements of temperature on a micrometer scale [69]. In addition, 2fFCS greatly reduces the dependency of FCS results on the size and shape of the excitation volume which due to optical saturation effects can vary significantly with excitation intensity. It is also less sensitive to slight changes in the refractive index [70], coverslip thickness, laser beam geometry, or optical saturation which can cause severe distortions of the confocal volume [43, 71] and, thus, can result in significant errors and misinterpretations in single focus FCS. The robustness of 2fFCS against optical and photophysical artifacts has been demonstrated for the investigation of systems with inherently large optical aberrations as they are often found in heterogeneous polymer systems [72]. However, when rather large colloids or macromolecules are used as probes for 2fFCS, their size with respect to the excitation laser focus has to be taken into account [73].

3.2 Total Internal Reflection FCS: Investigation of Interfaces

One of the challenges to investigate interfaces by FCS is the selective collection of the fluorescence emitted in the vicinity of the surface. The axial resolution of a confocal microscope results in averaging of the fluorescence emission within approx. 1 μm. As a consequence, surface effects are in most cases obscured in "normal" FCS measurements. With the evanescent wave of a laser beam totally reflected at the solid–liquid interface, however, the excitation can be restricted to a ca. 100 nm thin layer at the interface. This so-called total internal reflection FCS

(TIR-FCS) allows for an investigation of dynamic processes at liquid−solid interfaces [74–78]. Koynov and coworkers could for example measure diffusion coefficients of molecules and quantum dots at water−glass interfaces [77].

3.3 Superresolution in FCS

Superresolution microscopy methods have revolutionized optical microscopy within approx. the last two decades [79]. These methods can be separated in localization-based methods [80], which exploit the possibility to localize the isolated emission patterns of single molecules with high accuracy, and in methods which restrict the volume of excitation by stimulated emission. The latter can be combined with FCS resulting in STED-FCS (stimulated-emission-depletion FCS) [81, 82], where the excitation volume is minimized by an intensive donut-shaped STED laser pulse which depopulates basically all excited states except for a central volume of sub-diffraction size. This way, the spatial resolution Δd in lateral direction can be reduced to

$$\Delta d = \frac{\lambda}{2n \cdot \sin \alpha \sqrt{1 + \frac{I_{max}}{I_S}}} \tag{11}$$

where n is the refractive index, α the half of the opening angle of the collected light, λ and I_{max} are the wavelength and maximum intensity of the STED beam, and I_S represents the STED laser intensity at which the probability of fluorescence emission is reduced by half. STED-FCS has been used to study membrane dynamics [81, 83], but also found its way into polymer science. King et al. studied the mobility of end-labeled polystyrene chains in solutions of polystyrene in toluene near the polymer overlap concentration c^*. At concentrations higher than c^*, they found two modes of motion: self-diffusion and correlated segment fluctuations [84]. Leutenegger et al. went even one step further and combined STED-FCS with TIRF (see previous section) in order to achieve both high axial and lateral confinement reaching measurement volumes beyond 1 attoliter [85] (Fig. 4).

3.4 Temperature Control in FCS

Temperature is an important parameter which can significantly influence the properties and applicability of polymer systems. In order to capture all the interesting transitions in polymers, it is of considerable interest to be able to perform FCS measurements in polymers in an extended temperature range from cryogenic temperatures up to several hundred degrees centigrade with accurate temperature control and without artifacts from temperature gradients or convection. A setup

excitation
laser

$S_0 \rightarrow S_1$

+

STED
laser

$S_1 \rightarrow S_0$

→

fluorescence from
volume beyond
diffraction limit

$S_1 \rightarrow S_0 + h\nu$

Fig. 4 STED-FCS: The principle of STED-FCS

with high-temperature accuracy and stability has been reported by Müller et al. [86]
Elevated temperatures above ca. 80 °C can cause severe damages of the optical
components of the microscope due to heat transfer from the heating table. Flier
et al. [87] developed a heating device which allows for measurements at higher
temperatures of up to 150 °C using indium tin oxide (ITO) covered glass slides,
resistively heated by the application of a controlled voltage. This restricts the heated
mass to a minimum and therefore protects the optics from being overheated.

4 Limitations of FCS

4.1 Refractive Index Changes

FCS measurements possess some intrinsic limitations which should always be kept
in mind. One of the most severe pitfalls are refractive index changes which can
cause severe distortions of the confocal volume [43, 71, 88]. Such refractive index
changes can in particular appear in heterogeneous polymer systems where the
different compartments are composed of different polymers or solvents. The
distorted confocal volume causes failure of the equations typically used for the
FCS analysis which assume an ellipsoid shape of the confocal volume [see Eq. (2)].
Creating different models with the distorted volume is a hard or even impossible
task. Also the determination of diffusion coefficients using reference measurements
with the typical aqueous systems, i.e., Rh6G in water, will result in errors
[89]. Therefore, alternative calibration methods had to be found. Zettl et al. used
the known molecular weight dependence of the diffusion of rhodamine B (RhB)-
labeled polymer chains of different lengths in very dilute solution to determine the
size of the confocal volume and thus to calibrate the diffusion coefficient obtained

by FCS [90, 91]. The observation volume can also be calibrated using fluorescently labeled silica nanoparticles [92, 93] or dye-labeled polystyrene (PS) of known molecular mass [94], with the diffusion coefficient in dilute solution known from DLS measurements. One way to reduce the problems with distortions of the confocal volume is to measure at relatively small penetration depths of ca. 10 μm which is still reasonably far in the solution to avoid biased results due to influences of the interface. Another possibility to measure in systems with significant refractive index changes is dual-focus FCS as described in one of the previous sections [68]. Apart from the refractive index, slight changes in coverslip thickness, laser beam geometry, pinhole adjustment, or optical saturation can also lead to misinterpretations [43].

4.2 Spatial Resolution

The spatial resolution of FCS has been discussed in some papers [95, 96]. It has been stated that FCS is capable of resolving dynamics at the nanoscale, i.e., far beyond the limits of optical resolution [96]. On the other hand, it was mentioned that, as for all optical techniques, the diffraction limit has to be considered [95]. In general, it is possible to observe dynamics with a spatial accuracy beyond the diffraction limit of light. However, one has to be aware that, even though photon arrival times can be determined with picosecond accuracy, the obtained information about dynamics is averaged over time. This means dynamic heterogeneities which can be caused by mesh size fluctuations or fast structural changes cannot be observed directly and at the most could be estimated with an appropriate model explicitly implemented into the autocorrelation fit function. In addition, for the determination of spatially resolved diffusion coefficients from FCS measurements by changing the position of the focus, the diffraction limit determines the resolution. This can be only improved by superresolution techniques such as STED-FCS as states above.

4.3 Choice of the Fluorescent Probes

Just as for any other fluorescence microscopy technique, the choice of the fluorescent probe is of significant importance for FCS. Drops in the autocorrelations curves can occur as a result of photophysical and photochemical processes. In particular, the contribution of saturation effects and triplet blinking has been investigated [97, 98] and the rates of intersystem crossing and triplet decay as well as the excitation cross section of fluorophores could be determined [12]. In addition, antibunching is determined by the photophysics of the fluorophore. Therefore, the choice of appropriate dyes is essential to obtain meaningful results. Apart from that, the fluorescent probe should also serve as a selective label to

observe the diffusing species of interest. However, the interaction between dyes and polymer chains can also result in misinterpretations and should be carefully checked.

5 FCS in Polymer Solutions

FCS is a suitable technique to study polymer dynamics in solution, and the diffusional processes investigated by FCS provide important information about the local mechanical and viscoelastic properties of polymer solutions. Typically, a tiny amount of fluorescently labeled polymer chains or free dyes is added to the polymer solutions to be investigated or vice versa. This has not only the advantage of requiring minor amounts of fluorescent dyes or labeled polymers, but also minimizes the disturbance of the system by the introduced fluorophores.

One very interesting question concerning polymer solutions is how the diffusion of dye-labeled polymer chains and molecular probes changes with varying concentration and molecular weight of the probe and the surrounding. Principally, three different polymer concentration regimes can be distinguished: (i) dilute solutions in which diffusion is fully governed by the hydrodynamic radius of the diffusing species, (ii) semidilute solutions in which the polymer coils start to overlap, and (iii) concentrated solutions in which the chains strongly interact with each other. The border between the dilute and the semidilute regime is often called c^*, whereas the border between semidilute and concentrated regime is typically referred to as c^{**}. The semidilute and the concentrated solutions can be further divided into an unentangled and an entangled regime, the border of which is normally referred to as the entanglement concentration c_E. In the latter regime, topological constraints caused by entanglement dominate the dynamics. The transition between the regimes depends primarily on concentration and molecular weight of the polymer. In the following, the contributions of FCS to elucidate molecular dynamics in the various regimes will be discussed.

In this context, it is essential to discuss how the diffusion of single molecules or particles can be connected to the viscosity, if viscosity is a concept which still holds for length scales in the nanometer range. In fact, viscosity is a strong function of the length scale at which it is probed [99, 100], and already almost 30 years ago, the concept of length scale-dependent viscosity has been developed [101, 102]. Brochard and de Gennes suggested that the motion of a particle with a radius $R_0 \gg R_g$ (radius of gyration) is governed by the bulk viscosity [103]. As its size, however, becomes close to the tube diameter or smaller, the diffusion coefficient can increase dramatically by up to a few orders of magnitude. For entangled polymer solutions, this behavior is additionally governed by the entanglement spacing d_t (tube diameter) [104]. This was verified by diffusion measurements of particles with different diameter $2R_0$ which was comparable to the entanglement tube diameter using fluctuation correlation spectroscopy, i.e., correlation of the luminescence of gold nanoparticles after multiphoton excitation [105].

A similar approach was presented by Hołyst et al. who studied the diffusion of differently sized probes ranging from RhB molecules (1.7 nm) up to silica spheres (114 nm) in polyethylene glycol (PEG) solutions with a combination of FCS, capillary electrophoresis, and macroviscosity measurements (see Fig. 5) [106]. They found that the large probes diffused as expected from the macroviscosity of the solutions, whereas the diffusion of the small probes was clearly faster. As a consequence of this behavior, they distinguish between a macroviscosity experienced by larger probes and a nanoviscosity felt by small probes where the latter was observed to be up to a factor of 100 times smaller than the macroviscosity. A comparable result was also obtained for the diffusion of 2–44 nm sized probes in PVA solutions by Michelman-Ribeiro et al. [107]. The crossover from probing nanoviscosity to probing macroviscosity was found at a length scale at which the probe reached a size of approximately the radius of gyration of the polyethylene glycol (PEG) polymer under investigation [106]. It could be shown that the dependency of viscosity η on the ratio between an effective probe size and the correlation length ξ of the polymer follows a stretched exponential function. Probes smaller than the radius of gyration R_g of the polymer experience the nanoviscosity and the effective probe size is the probe radius R, whereas it equals the radius of gyration R_g for probe molecules of larger size which feel the macroviscosity of the polymer solution [106]. Thus,
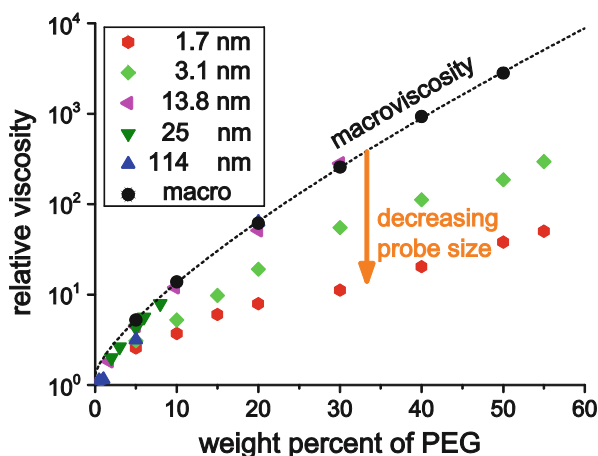

Fig. 5 Viscosity determined using diffusion measurements of differently sized probes in PEG 20000 solution. Small probes experience nanoviscosity, whereas large probes follow the macroviscosity which is shown as the *dashed black line* as a guide to the eye. The crossover length scale between nano- and macroviscosity in PEG20000 is larger than 3.1 nm and smaller than 13 nm (reproduced and adapted from Hołyst et al. [106] with permission of the PCCP Owner Societies)

$$\frac{\eta}{\eta_0} = \begin{cases} \dfrac{\eta_{\text{nano}}}{\eta_0} = \exp\left(b\left(\dfrac{R}{\xi}\right)^a\right) & \text{for} \quad R < R_{\text{g}} \\[2ex] \dfrac{\eta_{\text{macro}}}{\eta_0} = \exp\left(b\left(\dfrac{R_{\text{g}}}{\xi}\right)^a\right) & \text{for} \quad R > R_{\text{g}} \end{cases} \quad (12)$$

where the ratio between radius of gyration and correlation length ξ depends on the polymer concentration and the overlap concentration according to

$$\frac{R_{\text{g}}}{\xi} = \left(\frac{c}{c^*}\right)^\beta \quad (13)$$

where β depends on the Flory parameter v according to

$$\beta = -\frac{v}{(1 - 3 \cdot v)} \quad (14)$$

and for a three-dimensional polymer coil in a good solvent equals to ¾. Using the relationship shown in Eq. (12), all measured data of viscosity versus probe size could be plotted on one master curve. Furthermore, the parameter b in Equation (12) could be related to an excess activation energy for viscous flow compared to the one observed for pure solvent. The intrinsic viscosity was found to be directly proportional to this activation energy [108].

6 Diffusion of Small Molecular Probes

Small molecular probes sense the local viscosity and, therefore, no significant difference for their mobility in solutions of polymers of different (high) molecular weight is found. FCS measurements of the diffusion coefficients of a perylene monoimide dye for various concentrations of solutions of different molecular weight polystyrenes in acetophenone verified that all points fall onto the same master curve which could be fitted with a stretched exponential [109]. That means that from the perspective of the probes, the change in molecular weight of the polymer between 110 and 450 kg/mol does not seem to make a difference. At low polymer concentrations, the diffusion of the small probes is even not significantly influenced by the presence of polymer chains at all since it can diffuse basically unhindered through the polymer meshes. In a concentration range between ~6c^* and 20c^*, small molecules in polymer solutions were found to exhibit normal diffusion,[110] in contrast to larger nanoparticles for which a subdiffusive behavior was found (see below). The effect of the probe size on translational and rotational motion of perylene diimide derivatives of different size was monitored during the free radical bulk polymerization of styrene [54]. The increasing viscosity during bulk polymerization causes a drop in diffusion coefficient. The relative drop in rotational diffusion coefficient, i.e., the current diffusion coefficient D divided by

the diffusion coefficient D_0 in pure monomer solution (conversion $= 0$), was found to be similar for all probe sizes. All plots of D/D_0 versus the conversion showed the same behavior whereas significant differences were observed for the relative changes in the translational diffusion coefficient. The decrease in translational diffusion of the smallest dye resembles the rotational diffusion data. With respect to this scaling, the translational diffusion of the larger probes is significantly lowered, pointing to a change from probing nanoviscosity, apparently the property determining rotational diffusion, toward macroviscosity. A similar behavior was observed for the diffusion of the enzyme aldolase in aqueous solutions of polyethylene oxide. It was argued that the viscosity experienced for rotational motion is significantly reduced in comparison to the one experienced for translational motion due to entropic reasons [108].

Diffusion of small molecular probes was also studied in polymer melts. Herein, the diffusion of molecular tracers senses the glass transition temperature-dependent local segmental dynamics of the polymer matrix, rather than its macroscopic viscosity [111, 112]. The dependence of the diffusion coefficient on temperature could be fitted using a Vogel–Fulcher–Tammann function with an activation energy increasing with the tracer size and depending on the polymer. A combination of FCS and laser scanning confocal microscopy allowed for monitoring the dynamics of phase separation in a PS/poly(methyl phenyl siloxane) blend, two polymer components with a difference in glass transition temperature of more than 113 K and an upper critical solution temperature [113]. In polymer blends, the topology of the matrix polymer plays a pivotal role. Cherdhirankorn et al. observed significant differences in the diffusion of terrylene diimide probes in a polymer melt of linear and star-shaped 1,4-polyisoprenes, respectively [26]. FCS measurements are however not limited to small probes as will be shown in the following section.

7 Diffusion of Macromolecular Probes

Fluorescence-labeled polymer chains have been investigated by FCS to determine macromolecular diffusion in different polymer concentration regimes. Most studies were performed on labeled PS chains in toluene solutions of non-labeled PS of similar length.

For highly dilute and non-interacting solutions, this allows for the determination of self-diffusion coefficients D_0. Proceeding to the dilute regime where the polymer chains can interact with each other but still do not overlap, the dynamics is dominated by the hydrodynamic radius of the diffusing probe. According to the Kirkwood–Riseman theory [114], the diffusion coefficient can be calculated as follows:

$$D = D_0 - k_f \cdot c \tag{15}$$

where D_0 is the diffusion coefficient at infinite dilution (see above) and k_f is a

Fig. 6 Diffusion coefficient of labeled PS in toluene solutions as a function of polymer concentration and its prediction according to reptation and scaling theory (adapted with permission from Liu et al. [94]. Copyright 2005 American Chemical Society)
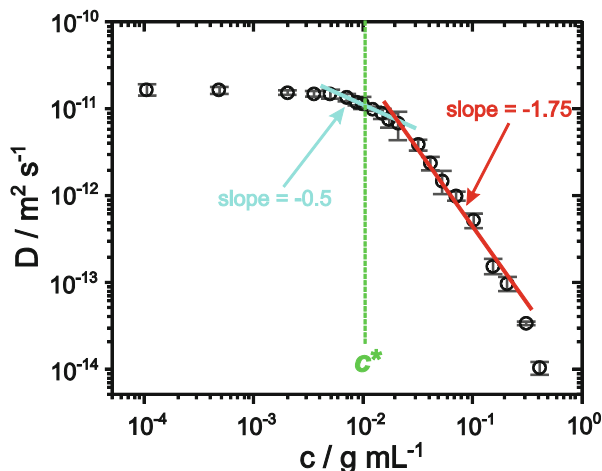
proportionality factor. This linear dependence of the diffusion coefficient on polymer concentration could be confirmed by the FCS measurements of Zettl et al. [90].

Further increase of the concentration above the overlap concentration c^* [115] causes a transition from the dilute to the semidilute regime. FCS measurements have verified that the concept of an overlap concentration is very useful as the plot of the diffusional correlation time versus the polymer concentration changes the slope at c^* [91]. In such a graph, linear fits of both regimes interact at the overlap concentration which depends on the molecular weight of the dissolved polymer chains. For increasing molecular mass, c^* shifts to lower concentrations. Fitting the dependency of c^* on molecular mass resulted in a Flory exponent of 0.59 in excellent agreement with the value of 0.588 predicted by theory for a polymer in a good solvent [116].

A very detailed study over a broad range of concentrations between 10^{-4} and 0.4 g/mL of high molecular weight PS chains ($M_W = 390$ kg/mol) in toluene was performed by Liu et al. [94]. In the dilute regime ($c < c^* \approx 0.01$ g/mL), they obtained basically a constant diffusion coefficient, i.e., $D \sim c^0$. Proceeding to the unentangled semidilute regime ($c^* \approx 0.01$ g/mL $< c < c_E \approx 0.02$ g/mL), where the polymer coils overlap but do not entangle effectively, a scaling of $D \sim c^{-1/2}$ in agreement with theory was determined [117]. When entanglements start to dominate the diffusional behavior at $c > c_E \approx 0.02$ g/mL, the scaling changes to $D \sim c^{-7/4}$ as predicted by basic scaling and reptation theory [115, 118]. The different regimes and their scaling behavior with polymer concentration are illustrated in the double-logarithmic plot in Fig. 6. FCS diffusion measurements of perylene-monoimide-labeled PS chains in unentangled and entangled semidilute solutions gave comparable results [109]. Additionally, in both of these studies, it was shown that the transition between the different regimes is rather smooth. In unentangled semidilute solutions of low molecular weight, the diffusion measurements of fluorescence-labeled polymer chains elucidate a linear dependency between viscosity and

temperature [58]. The activation energies obtained from Arrhenius fitting of these data for different polymer concentrations can be related to free volume theory [119].

Apart from the scaling of the diffusion coefficient of polymer chains with concentration, the dependency on their molecular weight is of high interest. For PS in the good solvent toluene, a scaling of $D \sim M^{-3/5}$ and $D \sim M^{-2}$ for dilute and semidilute entangled solutions was determined, respectively [24]. The question how the molecular weight of the surrounding chains depends on the diffusion coefficient of a small fraction of labeled PS chains in toluene has also been addressed [109]. It was found that higher molecular weights of the matrix polymer result in slower diffusion of the macromolecular probes as long as the molecular weight of the matrix does not exceed five times the molecular weight of the probe. For large matrix molecular weight, a master curve was obtained when plotting D normalized to the diffusion coefficient in infinite dilute solution versus the polymer concentration normalized to the overlap concentration of the diffusing fluorescently labeled polymer species. The obtained scaling parameters were -0.5 and -1.75 for the unentangled and entangled semidilute regime, respectively, in agreement with the previously mentioned study by Liu et al. [94]. In entangled polymer solutions, the motion of polymer chains is not independent from other chains anymore since the chains are coupled to each other through the entanglements. Therefore, in addition to self-diffusion, a collective diffusion mode could be observed in a semidilute solution of PS chains with a molecular weight of 515 kg/mol PS chains and a concentration of 13 wt [24]. This collective mode has a significant impact, for example, on the production of nanofibers [24].

For highly concentrated polymer solutions, FCS measurements revealed subdiffusive motion as an additional mode on an intermediate timescale between the fast collective diffusion and the slow self-diffusion [24]. In such slow systems, however, FCS reaches its limits when probe motion becomes so slow that the number of molecules moving into or out of the confocal volume within the measurement time is too small to allow for reliable statistics. Increasing the measurement time is often not straightforward since all fluorescence dyes have only a limited photostability. If a dye bleaches within the confocal volume, it will fake a faster diffusional motion than its real value. Therefore, for the study of such concentrated systems, wide-field fluorescence microscopy and subsequent single molecule tracking is a much better method [120] and has been utilized to study the glass transition [87, 121].

8 Diffusion of Nanoparticles in Polymers

As already discussed for molecular probes, the probe size plays a pivotal role for the analysis of polymer systems. Its size with respect to characteristic length scales of the investigated system determines the dynamics to be measured. For sufficiently large nanoparticles with diameters in the 100 nm range microviscosity can be

accessed. This technique is often referred to as passive microrheology [122–124]. In addition to its spatial resolution, the big advantage of microrheology is that only tiny sample volumes are required, a challenge for other rheometers.

Mukhopadhyay and coworkers observed the diffusion of differently sized gold nanoparticles (NPs) within an entangled liquid of poly(*n*-butyl methacrylate) (PBMA) above the glass transition temperature [105]. Instead of using a fluorescence signal for detection, they used the multiphoton absorption-induced luminescence of gold nanoparticles to perform fluctuation correlation spectroscopy measurement. One key parameter for the diffusion behavior is the ratio of particle size and tube diameter within the entangled polymer. Small nanoparticles can use this path to "sneak" through the polymer meshes whereas for larger particles Stokes–Einstein behavior is recovered. The size of the probes with respect to the mesh size also determines the diffusional mode of the nanoparticles. Small molecules or nanoparticles exhibit normal diffusion whereas anomalous diffusion was found for larger particles [110].

Slight anomalous diffusion is also observed for the motion of nanoparticles in agarose, i.e., polysaccharide, gels when its size amounts to approx. half of the critical size for which particles become trapped in the gel [32]. This behavior indicates that the diffusion through the gel of slightly larger mesh size than the particle diameter is hindered by the interactions of the saccharide which act as obstacles, but the particles can still jump from pore to pore. For nanoparticles of larger size, the connectivity of the pores decreases rapidly, and the particles get trapped because percolating paths for them become very rare.

9   FCS in Polymer Gels

This section will concentrate on FCS measurements in covalently (chemically) cross-linked polymer gels. The diffusion inside gels is affected by several parameters, in particular by the mesh size of the gel, its microstructure, the degree of swelling, the size of the diffusing species, and interactions between diffusing species and gel. At low polymer concentration, there is no significant difference between solutions of linear or cross-linked chains. Above a certain threshold concentration, the diffusion of stronger cross-linked gels decreases more rapidly when increasing the polymer concentration [125, 126]. This threshold concentration is, for example, approx. 3% w/v for PVA gels as shown by Michelman-Ribeiro et al. [127]. The cross-links act as obstacles for the diffusing species and affect their motion. This hindrance becomes more pronounced the higher the cross-link density and depends strongly on the size of the probe compared to the mesh size of the cross-linked polymer. Modesti et al. report that the most reasonable description for the diffusion in polymer networks is obtained by assuming that the cross-link effect is additive to the effective friction coefficient of the probes, i.e., the friction coefficient in the network equals the effective friction coefficient for the probe in the pure solvent plus a friction coefficient caused by the permanent cross-links

Fig. 7 Scaled characteristic diffusion time of fluorescent TAMRA molecules in PVA solutions and gels at several cross-link densities as a function of polymer concentration with linear fits. The times are scaled by the diffusion time of the probe in water. The *vertical dashed line* indicates the approximate gelation threshold (adapted from Michelman-Ribeiro et al. [127])
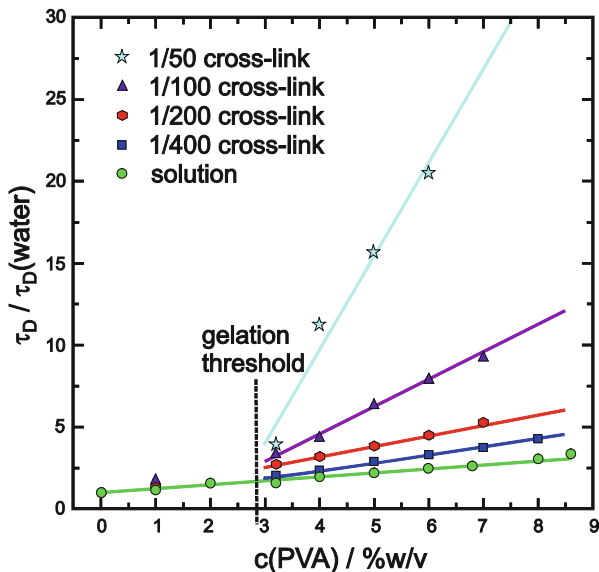
[125]. The description of polymers bearing very high cross-link densities with this model however fails, presumably due to pronounced swelling heterogeneities, i.e., the solvent preferably swells the more weakly cross-linked matrix and, thus, even at rather low degrees of swelling, opens up percolating regions of lower polymer density in which the dye can diffuse rather easily. Such an explanation is also underlined by our own observations on heterogeneous diffusion in polymer solutions during their cross-linking free radical bulk polymerization [128]. Interestingly, such a behavior is also observed for the linear bulk polymerization of MMA and is probably one of the main reasons for a pronounced Trommsdorff effect [129]. The change of diffusion behavior of three different proteins with hydrodynamic radii between 1 and 5 nm during swelling of cross-linked polyethyleneglycol networks hydrogel matrices with mesh sizes of ca. 14–19 nm can be explained by free volume theory [130]. A theory which explicitly considers the confinement a particle experiences from polymer chemical cross-links and which describes nanoparticle diffusion as subsequent activated hopping processes due to polymer network fluctuations has been recently published [131]. As already mentioned before, FCS is not only capable of studying the effect of cross-links in readily synthesized gels, but allows also for an investigation of the polymerization or cross-linking process itself. This way, the photo-crosslinking of PS microbeads with UV light was followed using FCS [132] (Fig. 7).

10 FCS in Charged Polymer Systems

Charges often play an important role for the properties of polymer systems. Therefore, it is not surprising that this topic was also addressed using FCS. Pristinski et al. investigated the translational diffusion of Alexa-labeled polymethacrylic acid in aqueous solution as a function of polymer concentration, solution pH, and ionic strength [133]. Below the overlap concentration $c*$ only minor changes were observed when varying the concentration. Beyond $c*$, the diffusion coefficients dropped significantly with increasing polymer concentration. A change from pH 5 to pH 8 resulted in an increased charge on the PMAA chains resulting in their twofold expansion. Enhanced ion concentrations of alkaline metal ions caused a chain contraction. Both dependencies could be detected using FCS diffusion measurements. Also the electrostatic interaction of oppositely charged polymers, in particular the complexation between negatively charged rhodamine-labeled oligonucleotides and cationic polymers, was studied [134]. The interaction of small (cationic) Rh6G dye molecules with (anionic) polystyrene sulfonate (PSS) polymers resulted in a fraction of free and a fraction of polymer-bound dye molecules [135]. The fraction of bound probes could be decreased by elevated salt levels indicating a dynamic exchange process between the free and bound cationic dyes. In another study, determination of the hydrodynamic radius of fluorescently labeled dextran could explain their solvent-dependent uptake into polyelectrolyte multilayer microcapsules [136]. FCS was also used to confirm the layer-by-layer assembly of PNIPAM microgel particles with (three) alternating layers of oppositely charged polymers as shown in Fig. 8 [137]. In general, a combination of simulations and theoretical studies with FCS measurements has a high potential to elucidate the effect of interaction in more detail. This is not only limited to charged species but can also take into account different interactions between polymer chains and probes [46].

11 FCS in Responsive Polymers

Responsive polymers have attracted considerable interest. Thermoresponsive systems which change their polarity and, thus, their shape and behavior within a physiological range between ca. 30 to 40 °C (see Fig. 9) have for example potential as drug delivery systems. Exploiting the potential of these polymers requires a detailed knowledge of their structure and dynamics at the nanoscopic and mesoscopic scale. The most studied responsive polymer, so far, has been poly(N-isopropylacrylamide) (PNIPAM) which exhibits a lower critical solution temperature (LCST) at around 32 °C. Below this temperature, PNIPAM chains in water are in a swollen state. At the LCST a volume phase transition occurs and the gel collapses and expels water. FCS allows for the investigation of the diffusion of small molecules and labeled PNIPAM chains in PNIPAM hydrogels. It was shown
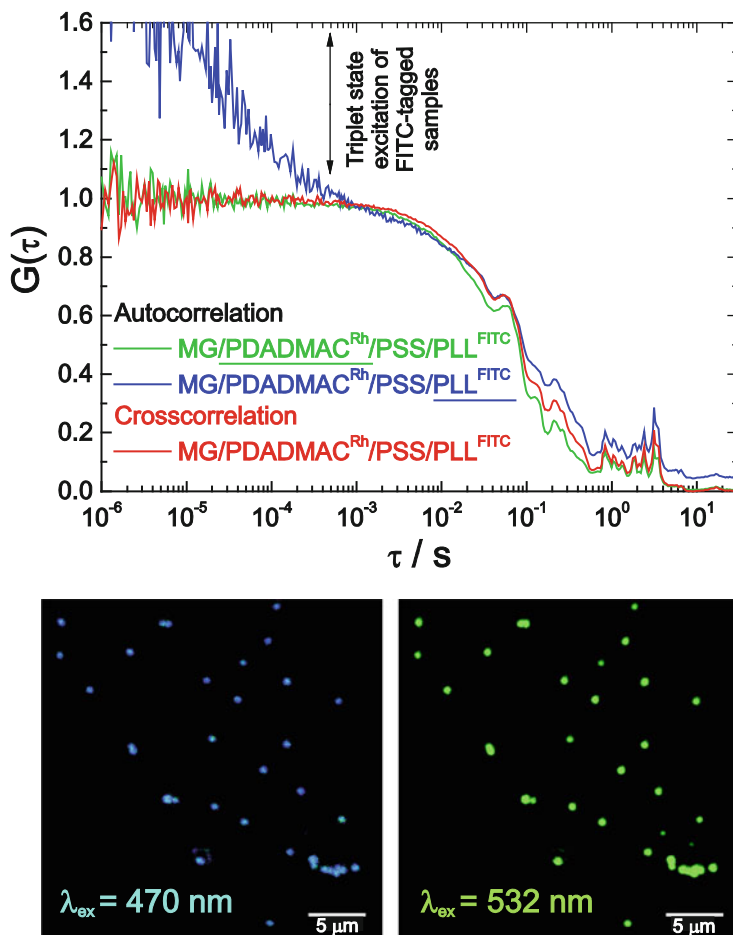
Fig. 8 FCS proves that the two differently labeled polyelectrolytes are anchored to the same PNIPAM microgel and, thus, that the layer-by-layer assembly has been successful. *Top*: Auto- and cross-correlation function of the coated PNIPAM nanoparticles. *Bottom*: Confocal fluorescence images of dried particles when excited at 470 nm (*left*) and 532 nm (*right*), respectively (adapted with permission from the Journal of Physical Chemistry [137]. Copyright (2007) American Chemical Society)

that the dependency of the diffusion coefficient on polymer concentration follows a stretched exponential [138]. Conventional hydrogels cross-linked with organic cross-linkers, however, suffer from severe disadvantages for technical and medical usage due to their low mechanical toughness, limited swelling ratio at equilibrium, and poor transparency. Clearly improved properties were reported for PNIPAM hydrogels cross-linked with clay nanoparticles [139]. These systems have also been studied by FCS using free probes [140] and covalent labeling of the clay nanoparticles [141]. In the latter case, FCS was used to verify the covalent labeling
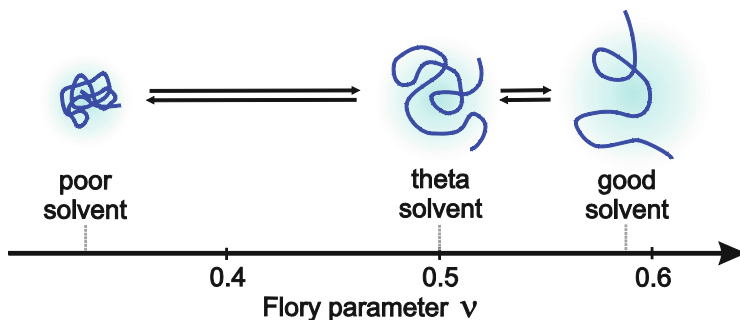
Fig. 9 Shapes and Flory parameters v of polymer chains in different solvent quality. The *three dotted lines* denote the theoretical values of v for different solvent qualities

and wide-field fluorescence microscopy studies revealed an anomalous diffusion of the clay nanoparticles in the hydrogels which significantly changed during the volume phase transition.

The temperature-induced change of mobility of differently sized probes through PNIPAM gels anchored to a solid substrate and, thus, with swelling restricted to one dimension was investigated by the Koynov group [126, 138]. In the swollen gel at low temperature, the small Alexa 647 probe exhibited a diffusion behavior which could be described with one diffusion coefficient, whereas the larger probe, green fluorescent protein (cylindrical shape with approx. $4.2 \times 2.4 \times 2.4$ nm^3[142]), significantly deviated from this single Fickian diffusion. Thus, the length scale of hindrance of probe motion due to the hydrogel structure is in a range between the sizes of both probes. In the transition regime from the swollen to the collapsed state around the volume phase transition temperature, two fractions of molecules with different diffusion coefficients were found for both dyes. This reflects the decreasing length scale of heterogeneous behavior of the probes caused by the denser polymer network which now also affects the diffusion of the small dye. After the collapse transition occurred at a swelling ratio of about 1.5, all dye molecules were expelled from the collapsed hydrogel films and thus moved freely outside of the polymer layer on the surface.

The diffusion of labeled dextrans in nanocomposites consisting of thermoresponsive PNIPAM microgels in a poly(acrylamide) hydrogel matrix could be measured with spatially resolved 2fFCS inside the microgel nanoparticles and in the surrounding hydrogel matrix [143]. The diffusion behavior of the probes in these nanocomposites depends on the cross-linking density of the microgels. For weakly cross-linked microgels, the nanocomposite forms an interpenetrating polymer network. As a consequence, swelling and deswelling of the microgel are obstructed and the mobility of embedded fluorescently labeled dextran probes is reduced. For highly cross-linked microgels, they collapse upon increasing the temperature above the volume phase transition temperature. This results in a heterogeneous swelling of the hydrogel matrix and the formation of pores near

Fig. 10 Flory exponents v as a function of the mol fraction x_{EtOH} of ethanol. The *three dotted lines* denote the theoretical values for the different solvent qualities as given in Fig. 9 (adapted with permission from Macromolecules [149]. Copyright (2012) American Chemical Society)
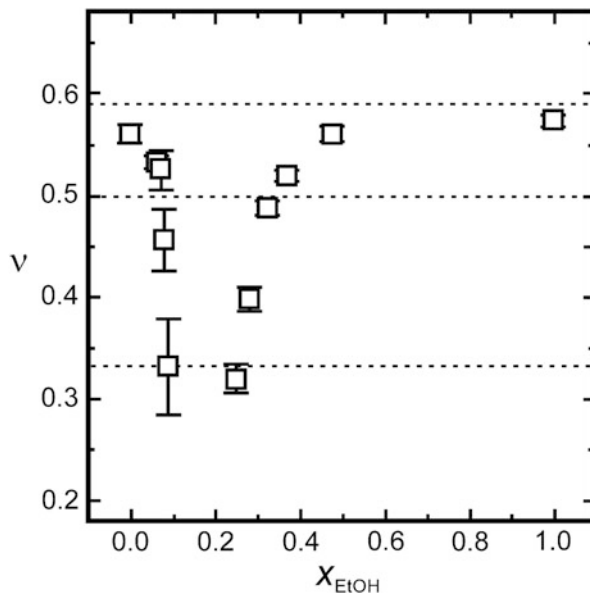
the surface of the microgels. Such behavior allows for tailoring of pore structures, thus enabling a control of the motion through these systems.

Amongst other polymers, PNIPAM exhibits a peculiar behavior in solvent mixtures. This polymer is, e.g., well soluble in water and in ethanol, but not in certain mixing ratios of these solvents. The reasons for this phenomenon called cononsolvency are still under discussion [144–147]. Cooperative hydration and competitive hydrogen bonding are current concepts to explain cononsolvency [148] Wang et al. applied FCS on fluorescently labeled PNIPAM of different degrees of polymerization and different water–ethanol compositions.[149] One technical challenge in these measurements was the change in refractive index upon addition of the cononsolvent ethanol to the aqueous polymer solution and the concomitant change in the confocal volume size and shape [43]. The change in refractive index was investigated using reference measurements of fluorescent nanoparticle diffusion in glycerol–water mixtures of known refractive indices by DLS. It was concluded that the effect of the refractive index mismatch and the consequential distortion of the confocal volume can be neglected for small distance of the focal point from the coverslip (ca. 10 μm is also in our view an appropriate distance for such measurements). From the diffusion times accessed by FCS, the hydrodynamic radii of the PNIPAM coils were determined for different polymer chain lengths and solvent mixtures. From the dependency of the hydrodynamic radius r_h on the polymer chain length N, the Flory scaling exponent [115] v was determined as $r_h \propto N^v$. As shown in Fig. 10, the values in pure ethanol and pure water are close to the predicted values for good solvents. In water–ethanol mixtures, the solvent quality for PNIPAM becomes significantly lower. Between a mole fraction x_{EtOH} of 0.09 and 0.25, no

uniform fluorescent signal could be detected in solution due to the (reversible) formation of suspended aggregates.

FCS studies were not only performed in PNIPAM, but also in thermoresponsive poly(2-oxazolines) [150] and to investigate the diffusion of nanoparticles in methylcellulose [151]. At low temperature, the latter exhibits a transient polymer mesh networks in the fluid state which at higher temperatures switches to a gelled state due to a formation of fibrillar structures.

Apart from using temperature for the switching, also other triggers such as pH, salt concentration, and solvent composition have been reported. Changes in pH value and ionic strength result in different interactions between polymer chains and between the probes and the polymers and are especially pronounced for charged species [133]. FCS studies at different humidity are sparse,[152] but may give a lot of interesting information about the changes of the polymer dynamics during swelling and deswelling.

12 FCS in Polymeric Systems Near Interfaces

The way that polymer chains diffuse at an interface is of high practical importance for example for coating applications. This question, however, turned out to be rather complex and measurements as well as theoretical considerations are challenging. The reason for this complexity are the numerous interactions and conformations that have to be considered at interfaces. A variation of FCS that is quite suitable to investigate surfaces is TIR-FCS where the sensitivity of FCS measurements at solid–liquid interfaces is significantly enhanced [76–78]. However, so far most FCS studies at interfaces have been performed in the "classical way."

It was, for example, found that end-labeled polyethylene glycol (PEG) chains adsorbed onto a hydrophobic self-assembled monolayer of octadecyltriethoxysilane coated onto a fused silica coverslip exhibit a flat "pancake" conformation due to significant adsorption of the polymer chains on the surface [60, 153]. This interaction causes that the diffusion coefficient scales with the number of chain segments according to a strong power law scaling with an exponent of $-3/2$, in contrast to the scaling of $-1/2$ in solution (see also Fig. 11). Not surprisingly, surface diffusion depends on surface coverage [154, 155]. At low surface coverages, an increase of the translational diffusion coefficient with increasing surface concentration was observed and attributed to a decrease of adsorption sites per molecule as chains switch from pancake to loop–train–tail conformation. When polymer chains start to overlap at the surface, the diffusion slows down significantly, due to crowding and entanglement with neighboring chains.

Translational diffusion within polymer brushes can be also accessed by FCS studies. It depends on the local viscosity within the brush and on probe size, thus causing different results for small and macromolecular probes [156]. For charged polymers, pH and ionic strength plays an additional role. If the dyes and the brushes are oppositely charged a dynamic association of dye molecules with the polymer

Fig. 11 Center-of-mass
diffusion coefficients D in
solution (*green circles*) and
at the surface (*blue squares*)
plotted against the degree of
polymerization N in double-
logarithmic scale. The
solution data can be well
fitted by a linear function
with a slope of $-1/2$. For
surface diffusion a slope of
$-3/2$ was obtained
(reproduced and adapted
with permission from
[60]. Copyright 2002
American Chemical
Society)
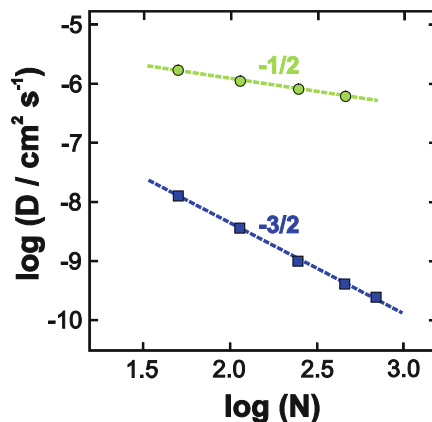
brush can be observed. The association and dissociation kinetics can be adjusted by
the pH or the addition of ions [157].

When the polymer brushes or surface coating are thermoresponsive, surfaces can
be also sensitive to temperature. Wang et al. studied lateral diffusion of fluores-
cently labeled polyelectrolyte poly(2-vinylpyridine) (P2VP) on the surface of
thermoresponsive poly(*N*-isopropylacrylamide) (PNIPAM) brushes [93]. At the
low pH used for the measurements, the P2VP chains were fully charged and thus
exhibited an extended coil conformation. Gradually increasing the temperature
resulted in an increase in the diffusion coefficient of the P2VP probes as expected
from the concomitant decrease of viscosity. However, at the volume phase transi-
tion temperature the diffusion coefficient started to decrease again. This behavior
was attributed to the collapse of the PNIPAM chain conformation changing the
hairy to a closely packed layer.

Apart from solid–liquid interfaces, also liquid–liquid interfaces can be investi-
gated using FCS. As an example, the adsorption dynamics of proteins at the oil–
water interface was measured [21]. However, changes in refractive index at the
interfaces should be carefully considered in order to avoid misinterpretations. A
thoughtful analysis of such effects has been performed by Donsmark et al. who
determined the molecular detection function of their system using numerical wave-
optical calculations [21].

13 FCS in Polymeric Micellar Systems

Polymeric amphiphiles can form different architectures such as spheres, disks, rods,
vesicles, or flocs [158]. For applications, it is of paramount importance to under-
stand how the shape and size of these assemblies varies with polymer concentra-
tion, quality of the solvent, and the lengths of the building blocks. FCS can

significantly contribute to solve these questions due to its capability to follow micellization and aggregation of polymers and detect their motion even at very low concentrations. Nörenberg et al. investigated the interaction of polymer and surfactant in solutions which can form mixed polymer–surfactant micelles. One of the main advantages using FCS was the very low concentration at which these measurement could be performed so that viscosity effects arising from interacting polymer tails and chains or Coulomb interactions could be neglected [159]. The majority of FCS studies in polymeric micellar systems, however, focus on the micellization and aggregation behavior of amphiphilic block copolymers which is expected to differ from common surfactants as the solvophobic and solvophilic parts of the molecule are much larger and also can be varied to a much greater extent.

Compared to other methods, the advantage of FCS is the ability to detect a very low critical micelle concentration [158, 160–163] (CMC) and a very low critical aggregation concentration [158, 160, 161] (CAC) as they often appear in block copolymer solutions. This could for example be demonstrated by Colombani et al. who could access the CMC of a diblock copolymers by FCS, but only obtained an upper estimate analyzing the absorption band of pyrene which is very sensitive to local polarity of its surrounding [162].

The principle of CMC or CAC measurements, respectively, by FCS is as follows. At concentrations below the CMC/CAC, the probes diffuse freely in solution and, therefore, FCS curves can be fitted with one correlation time. Once micelles or aggregates form, a fraction of the fluorescence probes will be implemented into the assemblies, whereas the remaining probes remain in solution. The fraction of probes in the assemblies diffuses significantly slower than the free probes in solution and will result in a longer diffusion time. Thus, the unimer concentration at which a fraction with a longer diffusion time appears in the autocorrelation curve can be defined as the CMC or CAC, respectively. Experimentally, this could be demonstrated by Bonné et al. [161]. Using rhodamine 6G as a fluorescence probe, they found that with increasing concentration of an amphiphilic poly(2-alkyl-2-oxazoline) diblock copolymer in water a second correlation time appeared at the CMC. The fraction of this correlation time reflecting the incorporated probe gradually increased with increasing polymer concentration. The two correlation times, however, remained constant, indicating that only the number of micelles but not their size increased.

For a correct determination of CMC or CAC, it is essential to know the interactions of the probe with the micelles or aggregates, respectively. Binding of the dye to the micelles/aggregates is always a dynamic equilibrium process. If the time constants of the binding and unbinding process, however, are in a time range similar to the duration that a dye on average requires to diffuse through the confocal volume, a mixture of both diffusion times will be measured. For higher micelle concentrations, the periods of free diffusion become shorter. Thus, even though the size of the micelles stays constant, the average time it takes a fluorescent probe to diffuse through the confocal volume becomes longer and the (time-averaged) diffusion coefficient smaller. Thus, as shown in Fig. 12, the hydrodynamic radius

Fig. 12 (Apparent) hydrodynamic radii r_h as determined by FCS on P [(NOx)10(MOx)32] with different tracers. *Squares*: solutions containing only labeled copolymers. *Triangles*: solutions containing both fluorescence-labeled and non-labeled copolymers. *Circles*: solutions containing non-labeled polymers and Rh6G (adapted from Colloid and Polymer Sci. [161]. Copyright (2007) Springer)
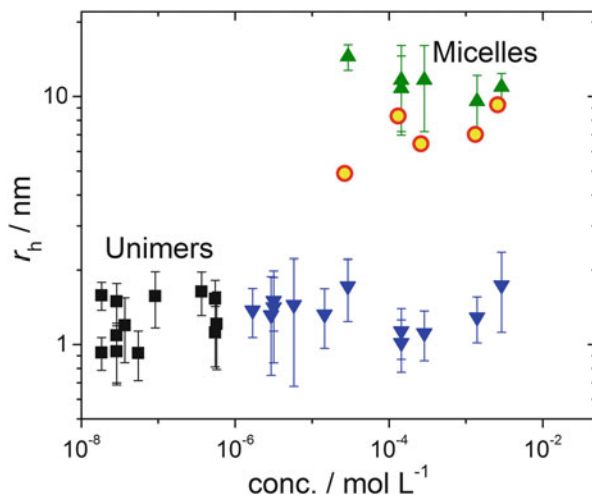
seems to grow with increasing polymer concentration, and the magnitude of this effect will depend on the equilibrium constant of binding of the dye to the micelle. As a consequence, despite the fact that the addition of a small amount of a low molar mass dye to the polymer solutions is a straightforward way of studying the aggregation of amphiphilic copolymers by FCS, great care has to be taken that the dyes show significant binding to the micelles. Otherwise, a wrong dependence of the hydrodynamic radii on polymer concentration will be observed, i.e., a too small radius will be obtained at low polymer concentration [161]. A good example for a suitable dye–polymer combination is octadecyl rhodamine B (ORB) which was found to be a suitable dye for probing the micellization of PS-poly(methyl acrylate) (PMA) block copolymers [164]. In this block copolymer, the ORB binds strongly to the core-shell interface of the PS-PMA micelles with its nonpolar aliphatic tail buried in and partially adsorbed to the PS core. The triplet quantum yield of ORB is basically negligible and, therefore, the corresponding parameters do not have to be implemented in the model for fitting the correlation curve. Another advantageous property of ORB is its self-quenching in water, in which the probe molecules are only weakly soluble and, thus, form aggregates. These ORB molecules show only weak fluorescence and do not significantly contribute to the monitored FCS fluctuations, thus lowering the background. As a consequence, the FCS fluctuations originate mainly from the ORB molecules bound to the core-shell interface of the PS-PMA micelles, increasing the sensitivity of this method.

Circumvention of the abovementioned problem of a dynamic binding equilibrium is possible using probes covalently attached to the copolymers. Even though this requires an often elaborate covalent labeling of the polymeric amphiphile, the results are nonambiguous [161]. Figure 12 shows that only two hydrodynamic radii are obtained, one corresponding to the unimers and the other representing the micelles. The fraction of the unimers gradually decreases whereas the one of the

micelles increases due to the increase of the number of micelles and therefore the probability of finding a labeled unimer in the micelle.

Apart from the determination of the CMC, the average size of micelles and aggregates [158, 160–162] can be studied using FCS. Combining Eq. (3) and the Stokes–Einstein equation (5), the hydrodynamic radius can be calculated from the diffusion time, if the size w_{xy} of the confocal volume is known. This size can be obtained by a reference measurement of a dye with known diffusion coefficient. A common and reliable reference is Rh6G in water with a diffusion coefficient 4.14×10^{-10} m^2 s^{-1} [71]. However, as already mentioned above, it should be checked that the binding behavior of the probing dye does not bias the results. Otherwise the hydrodynamic radius of the micelles might be misinterpreted to increase, i.e., micelles seem to grow with increasing monomer concentrations.

FCS studies on micellization and aggregation of polyoxazolines, an interesting polymer class due to their biocompatibility, non-toxicity, and immuno-response [165], have also been reported. The polarity of these polyoxazolines can be well adjusted by appropriate substitution with different alkyl groups, also allowing to tune their micellization and aggregation properties. In addition, polyoxazolines exhibit a lower critical solution temperature (LCST) which can also be tuned by appropriate substitution of the polymer backbone. Bonné et al. performed FCS using polyoxazolines covalently labeled at the end of the hydrophobic poly(2-n-nonyl-2-oxazoline) block or the hydrophilic poly(2-methyl-2-oxazoline) block, respectively, and found that the position of the label did not significantly influence micellization [161].

Polyoxazolines also exhibit a thermoresponsive aggregation behavior around the cloud point which could be investigated using a combination of FCS with varying temperature from r.t. up to ca. 50 °C, turbidimetry, and small-angle neutron scattering [150]. Different combinations of iso-propyl-(^{i}PrOx), n-propyl-(^{n}PrOx) and n-nonyl-(NOx) substituted polyoxazolines were investigated. Thermoresponsive P(^{i}PrOx) and P(^{n}PrOx) homopolymers show a behavior similar to the one encountered with other thermoresponsive homopolymers, such as PNIPAM [166], with the cloud point significantly depending on concentration and on the degree of polymerization, decreasing with increasing concentration and increasing degree of polymerization. At room temperature, both homopolymers were dissolved as unimers. At the cloud point (above 40 °C for P(^{i}PrOx) and 24–38 °C for P(^{n}PrOx)) the polymer chains collapsed and formed large aggregates (Fig. 13a). This aggregation process was fully reversible for P(^{i}PrOx) whereas the aggregates of P(^{n}PrOx) could not be fully dissolved upon cooling, presumably due to crystallization of the n-propyl side chains. The aggregation of the copolymers with a P^{i}PrOx and a P^{n}PrOx block was dominated by the behavior of P^{n}PrOx, the block with the lower cloud point. In this mixture, aggregates formed directly (Fig. 13b) at the cloud point of P^{n}PrOx. In gradient copolymers with, on average, 2 or 4 out of 50 iso-propyl side groups replaced by the very hydrophobic n-nonyl side group, a complex aggregation behavior was obtained due to the interplay between intra- and intermolecular association mediated by the hydrophobic ^{n}PrOx side chains. Already below the cloud point, aggregates formed due to the strong interaction of
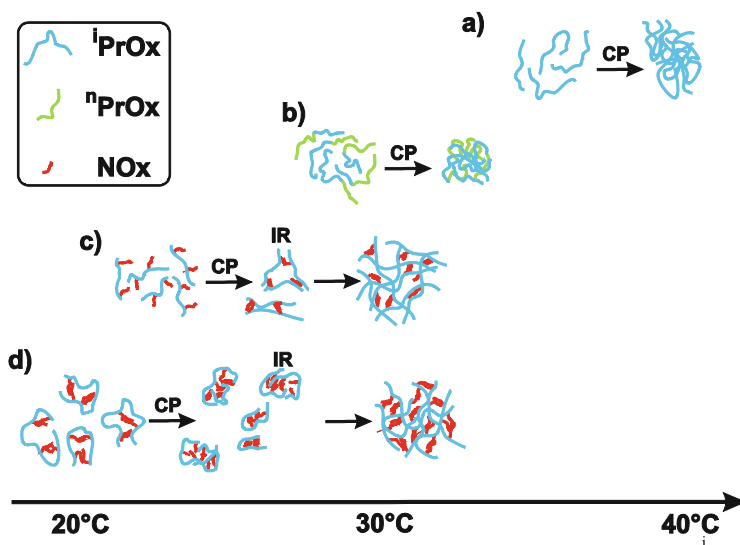
Fig. 13 Temperature-dependent aggregation behavior of (**a**) P(^{i}PrOx) homopolymers, (**b**) P (^{i}PrOx$_{25}$-b-^{n}PrOx$_{25}$) diblock copolymers, (**c**) P[^{i}PrOx$_{48}$NOx$_2$]$_{grad}$, and (**d**) P[^{i}PrOx$_{46}$NOx$_4$]$_{grad}$ gradient copolymers. The *different colors* indicate the different monomer types. CP stands for cloud point and IR for the intermediate regime (adapted from Colloid and Polymer Sci [150] Copyright (2012) Springer)

the strongly hydrophobic *n*-nonyl side groups (Fig. 13c, d). This effect was more pronounced for the gradient copolymers with a higher number of *n*-nonyl side groups. The hydrophobic interaction of these groups also shifts the collapse resulting in large aggregates to a few Kelvin above the cloud point. These aggregates, however, could not be detected with FCS, because sedimentation occurred due to their large size.

FCS is not only restricted to assembly studies of block copolymers and homopolymers, but also more complex aggregation systems can be analyzed. As an example, Štěpánek et al. investigated the solution behavior and self-assembly of a heteroarm star copolymer consisting of ca. 20 short PS and 20 long P2VP arms [167].

14 Comparison of FCS with Other Methods

Some observables that can be measured with FCS are in principle also accessible by other techniques. Thus, it is important to know the strengths and weaknesses of these methods with respect to FCS.

Dynamic light scattering (DLS, also known as photon correlation spectroscopy), for example, is an often used method to investigate the dynamics of particles,

micelles, and aggregates. The advantage of FCS, however, is the tiny amount of fluorescence probes required, which is approx. 3 orders of magnitude lower than the particle concentration in DLS [168]. Such small concentrations are of particular advantage for probing low micelle and aggregate concentrations. FCS also allows for the simultaneous detection of free dye, micelles, and large aggregates which is more difficult in DLS due to the fact that the scattered intensity is proportional to the particle mass and concentration [167]. Therefore, also small aggregates can be detected in the presence of large aggregates [160]. This advantage, however, disappears if the fluorescence signal is proportional to the particle or aggregate size, i.e., if a non-negligible amount of monomers or unimers are labeled. For polydisperse particles, micelles, or aggregates, it is important to keep in mind that FCS measures number-averaged molar masses (M_n) whereas weight-averaged molar masses (M_w) are obtained during DLS measurements [164].

Quasielastic neutron scattering (QENS) can detect diffusional processes at sub-nanometer length scales and with temporal resolution in picosecond time range [169]. In contrast to optical techniques, clearly higher spatial accuracy, however, comes along with a high technical demand, i.e., the necessity of a neutron source together with all its costs and security requirements. In addition, neutron scattering cross sections are ca. 10^9 times smaller than the absorption cross section of good fluorophores, resulting in long measuring times of hours. These long measuring times prohibit the scanning of many different sample areas and, thus, limit the imaging possibilities of QENS.

Combinations of FCS with DLS [158, 160, 163, 164], neutron scattering [150], or the application of all three techniques [170] to maximize the information about polymer systems have been successful.

15 FCS and Simulations

The combination of FCS with simulations in order to support the conclusions drawn from measurements bears a huge potential to gain a deeper understanding of dynamics in polymer systems. So far, only few such combined studies have been performed as discussed in a recent perspective article [171]. In contrast to measurements, different parameters can be well controlled and varied in simulations and interactions can be switched on and off. The comparison of the autocorrelation functions obtained from simulations under different assumptions with the measured FCS autocorrelation curves can subsequently point out the most appropriate model to describe polymer dynamics in different systems. One of the big challenges for FCS simulations is the large range of timescales which has to be accessed, typically from microseconds to seconds. The continuing development of computer technology helps to increase the time span and the number of particles which can be simulated with reasonable computational resources (CPU or GPU time, respectively). Yet, in order to cover the most interesting time range, even with the most powerful computational units the detailed level of the simulations has to be
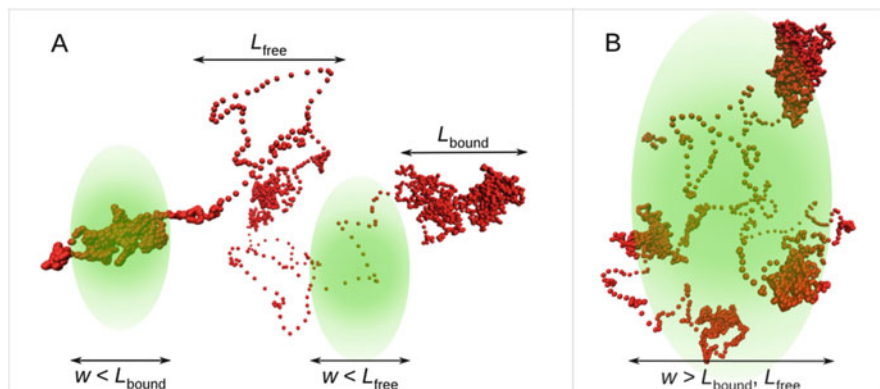
Fig. 14 Simulation of the trajectory of a tracer which can reversibly bind to polymer in a dilute polymer solution. When bound, the diffusion is strongly hindered whereas free diffusion is assumed in the non-bound periods. Panel (**a**) shows the case when the two length scales of the volumes with bound and unbound tracer are greater than the focal spot dimension, w, while panel (**b**) shows the opposite situation. In case (**a**), two distinct diffusion processes are resolved by FCS. In case (**b**), a single average process is observed. (adapted from Physical Review Letters [46] Copyright (2013) American Physical Society)

considerably reduced (coarse-graining) [172]. Such a simplification, however, can also bias the results calculated from the simulated data, and it is essential to carefully cross-check that the interpretations do not go beyond the approximations of the underlying model.

Concerning FCS, the most interesting observables from the simulations are the trajectories of single diffusion molecules or particles, respectively. From these trajectories, the mean square displacements and the autocorrelation functions can be calculated. This way, it can be analyzed how heterogeneity expresses itself in the FCS results, i.e., how anomalous diffusion is averaged over the relevant FCS time and length scales. Also, the question how interactions between dye and polymer chains influence FCS results has been recently addressed using a combination of FCS experiments with simulations [46] (Fig. 14).

16   Conclusion and Outlook

FCS has proven to be a suitable method for the investigation of dynamics in polymer systems. One of the main advantages consists in the high sensitivity of fluorescence detection, the potential to probe dynamics on a broad range of time-scales, and the possibility to measure in situ. Further development might focus on variation of local detection and, therefore, some kind of FCS imaging which allows to probe dynamics in different sample areas, e.g., inside and outside of gel and in the vicinity of gel surface. Also, improved labeling strategies and novel functional dyes are needed for example for a distinction of probes in areas of different polarity

or different local mobility. The limits of FCS are often set by the investigated systems which apart from bearing fluorescence impurities might scatter or refract light in an uncontrolled way at refractive index changes and therefore distort the confocal volume. The time resolution of scanning FCS approaches is limited by the period of time required to get sufficient photon counts in order to obtain reliable correlation functions. Despite these challenges, FCS has already contributed significantly to gain a deeper understanding of polymer physics. As shown in this book chapter, the studies so far focused mainly on diffusion of differently sized molecular and macromolecular probes in polymer solutions, classical and responsive polymer gels, polymer melts, glasses, and micellization, and aggregation systems. Combination of FCS with other experimental techniques or with simulations and theory will in future contribute to the establishment of FCS as a standard method to study polymer systems.

References

1. Wöll D (2014) Fluorescence correlation spectroscopy in polymer science. RSC Adv 4:2447–2465
2. Magde D, Webb WW, Elson E (1972) Thermodynamic fluctuations in a reacting system—Measurement by fluorescence correlation spectroscopy. Phys Rev Lett 29(11):705–708
3. Elson EL, Magde D (1974) Fluorescence correlation spectroscopy. 1. Conceptual basis and theory. Biopolymers 13(1):1–27
4. Magde D, Elson EL, Webb WW (1974) Fluorescence correlation spectroscopy. 2. Experimental realization. Biopolymers 13(1):29–61
5. Magde D, Webb WW, Elson EL (1978) Fluorescence correlation spectroscopy. 3. Uniform translation and laminar-flow. Biopolymers 17(2):361–376
6. Elson EL (2011) Fluorescence correlation spectroscopy: past, present, future. Biophys J 101(12):2855–2870
7. Haustein E, Schwille P (2007) Fluorescence correlation spectroscopy: novel variations of an established technique. Annu Rev Biophys Biomol Struct 36:151–169
8. Krichevsky O, Bonnet G (2002) Fluorescence correlation spectroscopy: the technique and its applications. Rep Prog Phys 65:251–297
9. Rigler R, Elson EL (eds) (2001) Fluorescence correlation spectroscopy. Theory and applications. Springer, Berlin, Heidelberg, New York
10. Schwille P (2001) Fluorescence correlation spectroscopy and its potential for intracellular applications. Cell Biochem Biophys 34:383–408
11. Rigler R, Mets Ü, Widengren J, Kask P (1993) Fluorescence correlation spectroscopy with high count rate and low-background—analysis of translational diffusion. Eur Biophys J 22(3):169–175
12. Widengren J, Mets Ü, Rigler R (1995) Fluorescence correlation spectroscopy of triplet-states in solution—a theoretical and experimental-study. J Phys Chem 99(36):13368–13379
13. Widengren J, Schwille P (2000) Characterization of photoinduced isomerization and back-isomerization of the cyanine dye Cy5 by fluorescence correlation spectroscopy. J Phys Chem A 104(27):6416–6428

14. Kask P, Piksarv P, Mets Ü (1985) Fluorescence correlation spectroscopy in the nanosecond time range: photon antibunching in dye fluorescence. Eur Biophys J 12:163–166

15. Sauer M, Hofkens J, Enderlein J (2011) Handbook of fluorescence spectroscopy and imaging—from single molecules to ensembles. Wiley-VCH, Weinheim

16. Laurence TA, Ly S, Bourguet F, Fischer NO, Coleman MA (2014) Fluorescence correlation spectroscopy at micromolar concentrations without optical nanoconfinement. J Phys Chem B 118(32):9662–9667

17. Müller CB, Loman A, Pacheco V, Koberling F, Willbold D, Richtering W, Enderlein J (2008) Precise measurement of diffusion by multi-color dual-focus fluorescence correlation spectroscopy. EPL 83(4):46001

18. Starchev K, Zhang J, Buffle J (1998) Applications of fluorescence correlation spectroscopy—particle size effect. J Colloid Interface Sci 203(1):189–196

19. Tcherniak A, Reznik C, Link S, Landes CF (2009) Fluorescence correlation spectroscopy: criteria for analysis in complex systems. Anal Chem 81:746–754

20. Sengupta P, Garai K, Balaji J, Periasamy N, Maiti S (2003) Measuring size distribution in highly heterogeneous systems with fluorescence correlation spectroscopy. Biophys J 84 (3):1977–1984

21. Donsmark J, Rischel C (2007) Fluorescence correlation spectroscopy at the oil – water interface: hard disk diffusion behavior in dilute β-lactoglobulin layers precedes monolayer formation. Langmuir 23(12):6614–6623

22. Shusterman R, Gavrinyov T, Krichevsky O (2008) Internal dynamics of superhelical DNA. Phys Rev Lett 100(9):098102

23. Winkler RG, Keller S, Rädler JO (2006) Intramolecular dynamics of linear macromolecules by fluorescence correlation spectroscopy. Phys Rev E 73(4):041919

24. Zettl U, Hoffmann ST, Koberling F, Krausch G, Enderlein J, Harnau L, Ballauff M (2009) Self-diffusion and cooperative diffusion in semidilute polymer solutions as measured by fluorescence correlation spectroscopy. Macromolecules 42(24):9537–9547

25. Banks DS, Fradin C (2005) Anomalous diffusion of proteins due to molecular crowding. Biophys J 89(5):2960–2971

26. Cherdhirankorn T, Floudas G, Butt H-J, Koynov K (2009) Effects of chain topology on the tracer diffusion in star polyisoprenes. Macromolecules 42:9183–9189

27. Masuda A, Ushida K, Okamoto T (2005) Direct observation of spatiotemporal dependence of anomalous diffusion in inhomogeneous fluid by sampling-volume-controlled fluorescence correlation spectroscopy. Phys Rev E 72(6):060101

28. Reitan NK, Juthajan A, Lindmo T, de Lange Davies C (2008) Macromolecular diffusion in the extracellular matrix measured by fluorescence correlation spectroscopy. J Biomed Opt 13 (5):054040–054040

29. Wachsmuth M, Waldeck W, Langowski J (2000) Anomalous diffusion of fluorescent probes inside living cell nuclei investigated by spatially-resolved fluorescence correlation spectroscopy. J Mol Biol 298(4):677–689

30. Weiss M, Elsner M, Kartberg F, Nilsson T (2004) Anomalous subdiffusion is a measure for cytoplasmic crowding in living cells. Biophys J 87(5):3518–3524

31. Saxton MJ (1995) Single-particle tracking: effects of corrals. Biophys J 69(2):389–398

32. Fatin-Rouge N, Starchev K, Buffle J (2004) Size effects on diffusion processes within agarose gels. Biophys J 86(5):2710–2719

33. Weiss M, Hashimoto H, Nilsson T (2003) Anomalous protein diffusion in living cells as seen by fluorescence correlation spectroscopy. Biophys J 84(6):4043–4052

34. Bernheim-Groswasser A, Shusterman R, Krichevsky O (2006) Fluorescence correlation spectroscopy analysis of segmental dynamics in actin filaments. J Chem Phys 125(8):084903

35. Kalkbrenner T, Arnold A, Tans SJ (2009) Internal dynamics of supercoiled DNA molecules. Biophys J 96(12):4951–4955

36. Petrov EP, Ohrt T, Winkler RG, Schwille P (2006) Diffusion and segmental dynamics of double-stranded DNA. Phys Rev Lett 97(25):258101

37. Shusterman R, Alon S, Gavrinyov T, Krichevsky O (2004) Monomer dynamics in double- and single-stranded DNA polymers. Phys Rev Lett 92(4):048303
38. Sokolov IM (2012) Models of anomalous diffusion in crowded environments. Soft Matter 8 (35):9043–9052
39. Ernst D, Köhler J, Weiss M (2014) Probing the type of anomalous diffusion with single-particle tracking. Phys Chem Chem Phys 16:7686–7691
40. Höfling F, Bamberg KU, Franosch T (2011) Anomalous transport resolved in space and time by fluorescence correlation spectroscopy. Soft Matter 7(4):1358–1363
41. Masuda A, Ushida K, Okamoto T (2005) New fluorescence correlation spectroscopy enabling direct observation of spatiotemporal dependence of diffusion constants as an evidence of anomalous transport in extracellular matrices. Biophys J 88(5):3584–3591
42. Masuda A, Ushida K, Okamoto T (2006) New fluorescence correlation spectroscopy (FCS) suitable for the observation of anomalous diffusion in polymer solution: time and space dependences of diffusion coefficients. J Photochem Photobiol A 183(3):304–308
43. Enderlein J, Gregor I, Patra D, Dertinger T, Kaupp UB (2005) Performance of fluorescence correlation spectroscopy for measuring diffusion and concentration. ChemPhysChem 6:2324–2336
44. Piskorz TK, Ochab-Marcinek A (2014) A universal model of restricted diffusion for fluorescence correlation spectroscopy. J Phys Chem B 118(18):4906–4912
45. Košovan P, Uhlík F, Kuldová J, Štěpánek M, Limpouchová Z, Procházka K, Benda A, Humpolíčková J, Hof M (2011) Monte Carlo simulation of fluorescence correlation spectroscopy data. Collect Czechoslov Chem Commun 76(3):207–222
46. Vagias A, Raccis R, Koynov K, Jonas U, Butt H-J, Fytas G, Košovan P, Lenz O, Holm C (2013) Complex tracer diffusion dynamics in polymer solutions. Phys Rev Lett 111 (8):088301
47. Hanbury Brown R, Twiss RQ (1956) Correlation between photons in 2 coherent beams of light. Nature 177(4497):27–29
48. Felekyan S, Kühnemuth R, Kudryavtsev V, Sandhagen C, Becker W, Seidel CAM (2005) Full correlation from picoseconds to seconds by time-resolved and time-correlated single photon detection. Rev Sci Instrum 76(8):083104
49. Wahl M, Rahn H-J, Gregor I, Erdmann R, Enderlein J (2007) Dead-time optimized time-correlated photon counting instrument with synchronized, independent timing channels. Rev Sci Instrum 78:033106
50. Widengren J, Mets Ü, Rigler R (1999) Photodynamic properties of green fluorescent proteins investigated by fluorescence correlation spectroscopy. Chem Phys 250(2):171–186
51. Ehrenberg M, Rigler R (1974) Rotational Brownian-motion and fluorescence intensity fluctuations. Chem Phys 4(3):390–401
52. Aragón SR, Pecora R (1975) Fluorescence correlation spectroscopy and Brownian rotational diffusion. Biopolymers 14(1):119–137
53. Aragón SR, Pecora R (1976) Fluorescence correlation spectroscopy as a probe of molecular-dynamics. J Chem Phys 64(4):1791–1803
54. Dorfschmid M, Müllen K, Zumbusch A, Wöll D (2010) Translational and rotational diffusion during radical bulk polymerization: a comparative investigation by full correlation fluorescence correlation spectroscopy (fcFCS). Macromolecules 43:6174–6179
55. Loman A, Gregor I, Stutz C, Mund M, Enderlein J (2010) Measuring rotational diffusion of macromolecules by fluorescence correlation spectroscopy. Photochem Photobiol Sci 2010 (9):627–636
56. Pieper CM, Enderlein J (2011) Fluorescence correlation spectroscopy as a tool for measuring the rotational diffusion of macromolecules. Chem Phys Lett 516(1-3):1–11
57. Berland KM, So PT, Gratton E (1995) Two-photon fluorescence correlation spectroscopy: method and application to the intracellular environment. Biophys J 68(2):694–701
58. Grabowski C, Mukhopadhyay A (2008) Diffusion of polystyrene chains and fluorescent dye molecules in semidilute and concentrated polymer solutions. Macromolecules 41:6191–6194

59. Schwille P, Haupts U, Maiti S, Webb WW (1999) Molecular dynamics in living cells observed by fluorescence correlation spectroscopy with one- and two-photon excitation. Biophys J 77(4):2251–2265

60. Sukhishvili SA, Chen Y, Müller JD, Gratton E, Schweizer KS, Granick S (2002) Surface diffusion of poly(ethylene glycol). Macromolecules 35(5):1776–1784

61. Zhao JJ, Bae SC, Xie F, Granick S (2001) Diffusion of polymer-coated nanoparticles studied by fluorescence correlation spectroscopy. Macromolecules 34(10):3123–3126

62. Dittrich PS, Schwille P (2002) Spatial two-photon fluorescence cross-correlation spectroscopy for controlling molecular transport in microfluidic structures. Anal Chem 74 (17):4472–4479

63. Schwille P, Meyer-Almes FJ, Rigler R (1997) Dual-color fluorescence cross-correlation spectroscopy for multicomponent diffusional analysis in solution. Biophys J 72 (4):1878–1886

64. Kügel W, Muschielok A, Michaelis J (2012) Bayesian-inference-based fluorescence correlation spectroscopy and single-molecule burst analysis reveal the influence of dye selection on DNA hairpin dynamics. ChemPhysChem 13(4):1013–1022

65. Ridgeway WK, Millar DP, Williamson JR (2012) The spectroscopic basis of fluorescence triple correlation spectroscopy. J Phys Chem B 116(6):1908–1919

66. Felekyan S, Kalinin S, Sanabria H, Valeri A, Seidel CA (2012) Filtered FCS: species auto- and cross-correlation functions highlight binding and dynamics in biomolecules. ChemPhysChem 13(4):1036–1053

67. Kühnemuth R, Seidel CAM (2001) Principles of single molecule multiparameter fluorescence spectroscopy. Single Mol 2(4):251–254

68. Dertinger T, Pacheco V, von der Hocht I, Hartmann R, Gregor I, Enderlein J (2007) Two-focus fluorescence correlation spectroscopy: a new tool for accurate and absolute diffusion measurements. ChemPhysChem 8(3):433–443

69. Müller CB, Weiss K, Loman A, Enderlein J, Richtering W (2009) Remote temperature measurements in femto-liter volumes using dual-focus-fluorescence correlation spectroscopy. Lab Chip 9(9):1248–1253

70. Pal N, Verma SD, Singh MK, Sen S (2011) Fluorescence correlation spectroscopy: an efficient tool for measuring size, size-distribution and polydispersity of microemulsion droplets in solution. Anal Chem 83(20):7736–7744

71. Dertinger T, Loman A, Ewers B, Müller CB, Kramer B, Enderlein J (2008) The optics and performance of dual-focus fluorescence correlation spectroscopy. Opt Express 16 (19):14353–14368

72. Müller CB, Eckert T, Loman A, Enderlein J, Richtering W (2009) Dual-focus fluorescence correlation spectroscopy: a robust tool for studying molecular crowding. Soft Matter 5 (7):1358–1366

73. Müller CB, Loman A, Richtering W, Enderlein J (2008) Dual-focus fluorescence correlation spectroscopy of colloidal solutions: Influence of particle size. J Phys Chem B 112 (28):8236–8240

74. Ivanov D, Shcheslavskiy V, Marki I, Leutenegger M, Lasser T (2009) High volume confinement in two-photon total-internal-reflection fluorescence correlation spectroscopy. Appl Phys Lett 94(8):083902–083903

75. Thompson NL, Burghardt TP, Axelrod D (1981) Measuring surface dynamics of biomolecules by total internal reflection fluorescence with photobleaching recovery or correlation spectroscopy. Biophys J 33(3):435–454

76. Thompson NL, Wang X, Navaratnarajah P (2009) Total internal reflection with fluorescence correlation spectroscopy: Applications to substrate-supported planar membranes. J Struct Biol 168(1):95–106

77. Yordanov S, Best A, Butt H-J, Koynov K (2009) Direct studies of liquid flows near solid surfaces by total internal reflection fluorescence cross-correlation spectroscopy. Opt Express 17(23):21149–21158

78. Yordanov S, Best A, Weisshart K, Koynov K (2011) An easy way to enable total internal reflection-fluorescence correlation spectroscopy (TIR-FCS) by combining commercial devices for FCS and TIR microscopy. Rev Sci Instrum 82:036105

79. Hell SW (2007) Far-field optical nanoscopy. Science 316(5828):1153–1158

80. Fürstenberg A, Heilemann M (2013) Single-molecule localization microscopy—near-molecular spatial resolution in light microscopy with photoswitchable fluorophores. Phys Chem Chem Phys 15(36):14919–14930

81. Eggeling C, Ringemann C, Medda R, Schwarzmann G, Sandhoff K, Polyakova S, Belov VN, Hein B, von Middendorff C, Schönle A, Hell SW (2009) Direct observation of the nanoscale dynamics of membrane lipids in a living cell. Nature 457(7233):1159–1162

82. Kastrup L, Blom H, Eggeling C, Hell SW (2005) Fluorescence fluctuation spectroscopy in subdiffraction focal volumes. Phys Rev Lett 94(17):178104

83. Mueller V, Honigmann A, Ringemann C, Medda R, Schwarzmann G, Eggeling C (2013) Chapter One - FCS in STED microscopy: studying the nanoscale of lipid membrane dynamics. In: Sergey YT (ed) Methods in enzymology, vol 519. Academic Press, New York, pp 1–38

84. King JT, Yu C, Wilson WL, Granick S (2014) Super-resolution study of polymer mobility fluctuations near c*. ACS Nano 8(9):8802–8809

85. Leutenegger M, Ringemann C, Lasser T, Hell SW, Eggeling C (2012) Fluorescence correlation spectroscopy with a total internal reflection fluorescence STED microscope (TIRF-STED-FCS). Opt Express 20(5):5243–5263

86. Müller CB, Richtering W (2008) Sealed and temperature-controlled sample cell for inverted and confocal microscopes and fluorescence correlation spectroscopy. Colloid Polym Sci 286 (11):1215–1222

87. Flier BMI, Baier MC, Huber J, Müllen K, Mecking S, Zumbusch A, Wöll D (2012) Heterogeneous diffusion in thin polymer films as observed by high-temperature single-molecule fluorescence microscopy. J Am Chem Soc 134(1):480–488

88. Hess ST, Webb WW (2002) Focal volume optics and experimental artifacts in confocal fluorescence correlation spectroscopy. Biophys J 83(4):2300–2317

89. Enderlein J, Gregor I, Patra D, Fitter J (2004) Art and artefacts of fluorescence correlation spectroscopy. Curr Pharm Biotechnol 5(2):155–161

90. Zettl H, Häfner W, Böker A, Schmalz H, Lanzendorfer M, Müller AHE, Krausch G (2004) Fluorescence correlation spectroscopy of single dye-labeled polymers in organic solvents. Macromolecules 37(5):1917–1920

91. Zettl H, Zettl U, Krausch G, Enderlein J, Ballauff M (2007) Direct observation of single molecule mobility in semidilute polymer solutions. Phys Rev E 75(6):061804

92. Koynov K, Mihov G, Mondeshki M, Moon C, Spiess HW, Müllen K, Butt HJ, Floudas G (2007) Diffusion and conformation of peptide-functionalized polyphenylene dendrimers studied by fluorescence correlation and 13C NMR spectroscopy. Biomacromolecules 8 (5):1745–1750

93. Wang W, Zhang C, Wang S, Zhao J (2007) Diffusion of single polyelectrolytes on the surface of poly(N-isopropylacrylamide) brushes. Macromolecules 40(26):9564–9569

94. Liu RG, Gao X, Adams J, Oppermann W (2005) A fluorescence correlation spectroscopy study on the self-diffusion of polystyrene chains in dilute and semidilute solution. Macromolecules 38(21):8845–8849

95. Enderlein J (2012) Polymer dynamics, fluorescence correlation spectroscopy, and the limits of optical resolution. Phys Rev Lett 108(10):108101

96. Krichevsky O (2013) Comment on "Polymer dynamics, fluorescence correlation spectroscopy, and the limits of optical resolution". Phys Rev Lett 110(15):159801

97. Davis LM, Shen G (2006) Accounting for triplet and saturation effects in FCS measurements. Curr Pharm Biotechnol 7(4):287–301

98. Widengren J, Rigler R, Mets Ü (1994) Triplet-state monitoring by fluorescence correlation spectroscopy. J Fluoresc 4(3):255–258

99. Won J, Onyenemezu C, Miller WG, Lodge TP (1994) Diffusion of spheres in entangled polymer solutions: a return to stokes-einstein behavior. Macromolecules 27(25):7389–7396

100. Ye X, Tong P, Fetters LJ (1998) Transport of probe particles in semidilute polymer solutions. Macromolecules 31(17):5785–5793

101. Dixon PK, Nagel SR, Weitz DA (1991) The length scale dependence of viscosity approaching the glass transition in glycerol. J Chem Phys 94(10):6924–6925

102. Kiyachenko YF, Litvinov YI (1985) Increase in scale length in a liquid as the glass transition temperature is approached. JETP Lett 42(5):266–269

103. Brochard Wyart F, De Gennes PG (2000) Viscosity at small scales in polymer melts. Eur Phys J E 1:93–97

104. Yamamoto U, Schweizer KS (2011) Theory of nanoparticle diffusion in unentangled and entangled polymer melts. J Chem Phys 135(22). doi:10.1063/1.3664863

105. Grabowski CA, Mukhopadhyay A (2014) Size effect of nanoparticle diffusion in a polymer melt. Macromolecules 47(20):7238–7242

106. Hołyst R, Bielejewska A, Szymanski J, Wilk A, Patkowski A, Gapinski J, Zywocinski A, Kalwarczyk T, Kalwarczyk E, Tabaka M, Ziebacz N, Wieczorek SA (2009) Scaling form of viscosity at all length-scales in poly(ethylene glycol) solutions studied by fluorescence correlation spectroscopy and capillary electrophoresis. Phys Chem Chem Phys 11 (40):9025–9032

107. Michelman-Ribeiro A, Horkay F, Nossal R, Boukari H (2007) Probe diffusion in aqueous poly(vinyl alcohol) solutions studied by fluorescence correlation spectroscopy. Biomacromolecules 8(5):1595–1600

108. Wiśniewska A, Sozański K, Kalwarczyk T, Kędra-Królik K, Pieper C, Wieczorek SA, Jakieła S, Enderlein J, Hołyst R (2014) Scaling of activation energy for macroscopic flow in poly(ethylene glycol) solutions: entangled—non-entangled crossover. Polymer 55 (18):4651–4657

109. Cherdhirankorn T, Best A, Koynov K, Peneva K, Müllen K, Fytas G (2009) Diffusion in polymer solutions studied by fluorescence correlation spectroscopy. J Phys Chem B 113:3355–3359

110. Omari RA, Aneese AM, Grabowski CA, Mukhopadhyay A (2009) Diffusion of nanoparticles in semidilute and entangled polymer solutions. J Phys Chem B 113(25):8449–8452

111. Best A, Pakula T, Fytas G (2005) Segmental dynamics of bulk polymers studied by fluorescence correlation spectroscopy. Macromolecules 38(10):4539–4541

112. Cherdhirankorn T, Harmandaris V, Juhari A, Voudouris P, Fytas G, Kremer K, Koynov K (2009) Fluorescence correlation spectroscopy study of molecular probe diffusion in polymer melts. Macromolecules 42(13):4858–4866

113. Doroshenko M, Gonzales M, Best A, Butt H-J, Koynov K, Floudas G (2012) Monitoring the dynamics of phase separation in a polymer blend by confocal imaging and fluorescence correlation spectroscopy. Macromol Rapid Commun 33(18):1568–1573

114. Kirkwood JG, Riseman J (1948) The intrinsic viscosities and diffusion constants of flexible macromolecules in solution. J Chem Phys 16(6):565–573

115. de Gennes P-G (1979) Scaling concepts in polymer physics. Cornell University Press, London

116. Rubinstein M, Colby RH (2003) Polymer physics. Oxford University Press, Oxford

117. Hess W (1986) Self-diffusion and reptation in semidilute polymer solutions. Macromolecules 19(5):1395–1404

118. Doi M, Edwards DA (1986) The theory of polymer dynamics. Oxford University Press, New York

119. Vrentas JS, Duda JL (1977) Diffusion in polymer-solvent systems. 2. Predictive theory for dependence of diffusion-coefficients on temperature, concentration, and molecular-weight. J Polym Sci B 15(3):417–439

120. Wöll D, Kölbl C, Stempfle B, Karrenbauer A (2013) Novel method for automatic single molecule tracking of blinking molecules at low intensities. Phys Chem Chem Phys 15:6196–6205
121. Orrit M (2013) Towards a molecular view of glass heterogeneity. Angew Chem Int Ed 52 (1):163–166
122. Joly L, Ybert C, Bocquet L (2006) Probing the nanohydrodynamics at liquid-solid interfaces using thermal motion. Phys Rev Lett 96(4):046101
123. Rathgeber S, Beauvisage HJ, Chevreau H, Willenbacher N, Oelschlaeger C (2009) Microrheology with fluorescence correlation spectroscopy. Langmuir 25(11):6368–6376
124. Solomon MJ, Lu Q (2001) Rheology and dynamics of particles in viscoelastic media. Curr Opin Colloid Interface Sci 6(5-6):430–437
125. Modesti G, Zimmermann B, Börsch M, Herrmann A, Saalwächter K (2009) Diffusion in model networks as studied by NMR and fluorescence correlation spectroscopy. Macromolecules 42(13):4681–4689
126. Raccis R, Roskamp R, Hopp I, Menges B, Koynov K, Jonas U, Knoll W, Butt HJ, Fytas G (2011) Probing mobility and structural inhomogeneities in grafted hydrogel films by fluorescence correlation spectroscopy. Soft Matter 7(15):7042–7053
127. Michelman-Ribeiro A, Boukari H, Nossal R, Horkay F (2004) Structural changes in polymer gels probed by fluorescence correlation spectroscopy. Macromolecules 37(26):10212–10214
128. Wöll D, Uji-i H, Schnitzler T, Hotta J, Dedecker P, Herrmann A, De Schryver FC, Müllen K, Hofkens J (2008) Radical polymerization tracked by single molecule spectroscopy. Angew Chem Int Ed 47:783–787
129. Stempfle B, Dill M, Winterhalder M, Müllen K, Wöll D (2012) Single molecule diffusion and its heterogeneity during the bulk radical polymerization of styrene and methyl methacrylate. Polym Chem 3:2456–2463
130. Zustiak SP, Boukari H, Leach JB (2010) Solute diffusion and interactions in cross-linked poly (ethylene glycol) hydrogels studied by fluorescence correlation spectroscopy. Soft Matter 6 (15):3609–3618
131. Dell ZE, Schweizer KS (2014) Theory of localization and activated hopping of nanoparticles in cross-linked networks and entangled polymer melts. Macromolecules 47(1):405–414
132. Zhang R, Cherdhirankorn T, Graf K, Koynov K, Berger R (2008) Swelling of cross-linked polystyrene beads in toluene. Microelectron Eng 85(5–6):1261–1264
133. Pristinski D, Kozlovskaya V, Sukhishvili SA (2005) Fluorescence correlation spectroscopy studies of diffusion of a weak polyelectrolyte in aqueous solutions. J Chem Phys 122 (1):014907
134. van Rompaey E, Engelborghs Y, Sanders N, De Smedt C, Demeester J (2001) Interactions between oligonucleotides and cationic polymers investigated by fluorescence correlation spectroscopy. Pharm Res 18(7):928–936
135. Jia P, Yang Q, Gong Y, Zhao J (2012) Dynamic exchange of counterions of polystyrene sulfonate. J Chem Phys 136(8):084904
136. Kim B-S, Lebedeva OV, Koynov K, Gong H, Glasser G, Lieberwith I, Vinogradova OI (2005) Effect of organic solvent on the permeability and stiffness of polyelectrolyte multilayer microcapsules. Macromolecules 38(12):5214–5222
137. Wong JE, Müller CB, Laschewsky A, Richtering W (2007) Direct evidence of layer-by-layer assembly of polyelectrolyte multilayers on soft and porous temperature-sensitive PNiPAM microgel using fluorescence correlation spectroscopy. J Phys Chem B 111(29):8527–8531
138. Gianneli M, Beines PW, Roskamp RF, Koynov K, Fytas G, Knoll W (2007) Local and global dynamics of transient polymer networks and swollen gels anchored on solid surfaces. J Phys Chem C 111(35):13205–13211
139. Haraguchi K, Takehisa T (2002) Nanocomposite hydrogels: a unique organic–inorganic network structure with extraordinary mechanical, optical, and swelling/de-swelling properties. Adv Mater 14(16):1120–1124

140. Ferse B, Richter S, Eckert F, Kulkarni A, Papadakis CM, Arndt KF (2008) Gelation mechanism of poly(N-isopropylacrylamide)-clay nanocomposite hydrogels synthesized by photopolymerization. Langmuir 24(21):12627–12635

141. Stempfle B, Große A, Ferse B, Arndt K-F, Wöll D (2014) Anomalous diffusion in thermoresponsive polymer-clay composite hydrogels probed by widefield fluorescence microscopy. Langmuir. doi:10.1021/la503571j

142. Hink MA, Griep RA, Borst JW, van Hoek A, Eppink MHM, Schots A, Visser AJWG (2000) Structural dynamics of green fluorescent protein alone and fused with a single chain Fv protein. J Biol Chem 275(23):17556–17560

143. Lehmann S, Seiffert S, Richtering W (2012) Spatially resolved tracer diffusion in complex responsive hydrogels. J Am Chem Soc 134:15963–15969

144. Ebeling B, Eggers S, Hendrich M, Nitschke A, Vana P (2014) Flipping the pressure- and temperature-dependent cloud-point behavior in the cononsolvency system of poly (N-isopropylacrylamide) in water and ethanol. Macromolecules 47(4):1462–1469

145. Hofmann CH, Plamper FA, Scherzinger C, Hietala S, Richtering W (2013) Cononsolvency revisited: solvent entrapment by N-Isopropylacrylamide and N N-diethylacrylamide microgels in different water/methanol mixtures. Macromolecules 46(2):523–532

146. Kyriakos K, Philipp M, Adelsberger J, Jaksch S, Berezkin AV, Lugo DM, Richtering W, Grillo I, Miasnikova A, Laschewsky A, Müller-Buschbaum P, Papadakis CM (2014) Cononsolvency of water/methanol mixtures for PNIPAM and PS-b-PNIPAM: pathway of aggregate formation investigated using time-resolved SANS. Macromolecules 47 (19):6867–6879

147. Maccarone S, Scherzinger C, Holderer O, Lindner P, Sharp M, Richtering W, Richter D (2014) Cononsolvency effects on the structure and dynamics of microgels. Macromolecules: 140820073721000. doi:10.1021/ma500954t

148. Tanaka F, Koga T, Kojima H, Winnik FM (2009) Temperature- and tension-induced coil − globule transition of poly(N-isopropylacrylamide) chains in water and mixed solvent of water/methanol. Macromolecules 42(4):1321–1330

149. Wang F, Shi Y, Luo S, Chen Y, Zhao J (2012) Conformational transition of poly (N-isopropylacrylamide) single chains in its cononsolvency process: a study by fluorescence correlation spectroscopy and scaling analysis. Macromolecules 45(22):9196–9204

150. Salzinger S, Huber S, Jaksch S, Busch P, Jordan R, Papadakis CM (2012) Aggregation behavior of thermo-responsive poly(2-oxazoline)s at the cloud point investigated by FCS and SANS. Colloid Polym Sci 290(5):385–400

151. Jee A-Y, Curtis-Fisk JL, Granick S (2014) Nanoparticle diffusion in methycellulose thermoreversible association polymer. Macromolecules 47(16):5793–5797

152. Fu Y, Ye F, Sanders WG, Collinson MM, Higgins DA (2006) Single molecule spectroscopy studies of diffusion in mesoporous silica thin films. J Phys Chem B 110(18):9164–9170

153. Sukhishvili SA, Chen Y, Müller JD, Gratton E, Schweizer KS, Granick S (2000) Materials science—diffusion of a polymer 'pancake'. Nature 406(6792):146–146

154. Zhao J, Granick S (2004) Polymer lateral diffusion at the solid − liquid interface. J Am Chem Soc 126(20):6242–6243

155. Zhao J, Granick S (2007) How polymer surface diffusion depends on surface coverage. Macromolecules 40(4):1243–1247

156. Pan X, Aw C, Du Y, Yu H, Wohland T (2006) Characterization of poly(acrylic acid) diffusion dynamics on the grafted surface of poly(ethylene terephthalate) films by fluorescence correlation spectroscopy. Biophys Rev Lett 1(4):1–9

157. Reznik C, Estillore N, Advincula RC, Landes CF (2009) Single molecule spectroscopy reveals heterogeneous transport mechanisms for molecular ions in a polyelectrolyte polymer brush. J Phys Chem B 113(44):14611–14618

158. Schuch H, Klingler J, Rossmanith P, Frechen T, Gerst M, Feldthusen J, Müller AHE (2000) Characterization of micelles of polyisobutylene-block-poly(methacrylic acid) in aqueous medium. Macromolecules 33(5):1734–1740

159. Nörenberg R, Klingler J, Horn D (1999) Study of the interactions between poly(vinyl pyrrolidone) and sodium dodecyl sulfate by fluorescence correlation spectroscopy. Angew Chem Int Ed 38(11):1626–1629
160. Bonné TB, Lüdtke K, Jordan R, Štěpánek P, Papadakis CM (2004) Aggregation behavior of amphiphilic poly(2-alkyl-2-oxazoline) diblock copolymers in aqueous solution studied by fluorescence correlation spectroscopy (vol 282, pg 833, 2004). Colloid Polym Sci 282 (12):1425–1425
161. Bonné TB, Papadakis CM, Lüdtke K, Jordan R (2007) Role of the tracer in characterizing the aggregation behavior of aqueous block copolymer solutions using fluorescence correlation spectroscopy. Colloid Polym Sci 285(5):491–497
162. Colombani O, Ruppel M, Schubert F, Zettl H, Pergushov DV, Müller AHE (2007) Synthesis of poly(n-butyl acrylate)-block-poly(acrylic acid) diblock copolymers by ATRP and their micellization in water. Macromolecules 40(12):4338–4350
163. Loos K, Böker A, Zettl H, Zhang M, Krausch G, Müller AHE (2005) Micellar aggregates of amylose-block-polystyrene rod – coil block copolymers in Water and THF. Macromolecules 38(3):873–879
164. Humpolíčková J, Procházka K, Hof M, Tuzar Z, Špírková M (2003) Fluorescence correlation spectroscopy using octadecylrhodamine B as a specific micelle-binding fluorescent tag; light scattering and tapping mode atomic force microscopy studies of amphiphilic water-soluble block copolymer micelles†,‡. Langmuir 19(10):4111–4119
165. Sedlacek O, Monnery BD, Filippov SK, Hoogenboom R, Hruby M (2012) Poly(2-Oxazoline)s—are they more advantageous for biomedical applications than other polymers? Macromol Rapid Commun 33(19):1648–1662
166. Okada Y, Tanaka F (2005) Cooperative hydration, chain collapse, and flat LCST behavior in aqueous poly(N-isopropylacrylamide) solutions. Macromolecules 38(10):4465–4471
167. Štěpánek M, Matějíček P, Humpolíčková J, Havránková J, Podhájecká K, Špírková M, Tuzar Z, Tsitsilianis C, Procházka K (2005) New insights on the solution behavior and self-assembly of polystyrene/poly(2-vinylpyridine) 'hairy' heteroarm star copolymers with highly asymmetric arms in polar organic and aqueous media. Polymer 46(23):10493–10505
168. Jurkiewicz P, Koňák Č, Šubr V, Hof M, Štěpánek P, Ulbrich K (2008) Investigation of nanoparticle coating by fluorescence correlation spectroscopy. Macromol Chem Phys 209 (14):1447–1453
169. Roe RJ (2000) Methods of X-Ray and neutron scattering in polymer science (Topics in polymer science). Oxford University Press, New York
170. Malo de Molina P, Appavou M-S, Gradzielski M (2014) Oil-in-water microemulsion droplets of TDMAO/decane interconnected by the telechelic C18-EO150-C18: clustering and network formation. Soft Matter 10(28):5072–5084
171. Papadakis CM, Košovan P, Richtering W, Wöll D (2014) Polymers in focus: fluorescence correlation spectroscopy. Colloid Polym Sci 292:2399–2411
172. Peter C, Kremer K (2009) Multiscale simulation of soft matter systems—from the atomistic to the coarse-grained level and back. Soft Matter 5(22):4357–4366